Comparison of surface wave techniques to estimate shear wave velocity in a sand and gravel sequence: Holme-Pierrepont, Nottingham, UK

Gunn* D.A., Williams, G., Raines, M.G., Busby, J.P., Williams, J.D.O. & Pearson, S.G.

British Geological Survey, Kingsley Dunham Centre, Keyworth, Nottingham, NG12 5GG

*** Corresponding author – David Gunn dgu@bgs.ac.uk**

Abstract

The aims of this study were to evaluate some surface wave methods and their limitations with regard to aggregate variability and thickness determinations. We compared the results of field assessments of sand and gravel sequences using different surface wave survey approaches. The first, followed a seismic refraction approach, the second, a continuous surface wave (CSW) survey methodology, and the third, adopted a multi-channel analysis of surface waves (MASW) technique to the original refraction field setup and records. The sand and gravel sequences were highly heterogeneous and the shear wave profiles were not normally dispersive, which had a significant effect upon the performance of the different field approaches. Neither the thickness nor the internal structure could be adequately characterised using surface wave approaches. Information over a broad spectrum from which velocity-depth profiles were produced was provided via both CSW and MASW approaches, but the upper frequency of operation was limited in both methods because of poorer signal quality at higher frequencies. Further probing using an ultra-lightweight cone penetrometer, continuous reflection profiling using ground penetration radar and also, an active extraction programme at the field site provided the opportunity to directly observe the subsurface geology and verify field results. Within the sand and gravel sequence, high velocity layers were associated with matrix supported coarse gravel lenses, some of which were weakly cemented. Shear wave velocity profiles obtained using vertically vibrating sources during CSW surveys were different to profiles obtained using a horizontally polarised sources in the refraction survey. This was attributed to different propagation paths and modes of propagation, but could also be attributed to data inversion methods.

Introduction

In many ground assessments such as, earthworks condition (Zagyapan & Fairfield 2002, Gunn *et al.* 2005, 2006a, 2007), aggregate resource (Gunn *et al.* 2006b) and seismic amplification (Murphy *et al.* 1971, Seed *et al.* 1997) it is necessary to characterise near-surface heterogeneity in terms of materials, their distribution and engineering properties. Information on the near surface variability can be provided via several means, such as invasive probing using cone penetration resistance tests (CPT) (Butcher & Powell 1996 & Langton 1999) and standard penetration test (SPT) (Skempton 1986, Liao & Whitman 1986 & Clayton 1990) methods, cross-hole techniques (Jackson & McCann 1997 & Jackson *et al.* 2001) or rapid, surface methods (Gunn 2006b). Penetration of coarse, granular materials is especially challenging, and thus, invasive probe and borehole based methods can become time consuming and costly. However, surface wave surveys can be quickly mobilised to provide shear wave velocity and thus shear modulus information, from which material heterogeneity can be assessed.

Particle motion contributing to the surface wave propagation at the near surface changes with depth in a way that is related to the wavelength (Bullen 1963 & Richart *et al.* 1970). Surface waves are dispersive, which results in the velocity of wave propagation, called the phase velocity, changing with frequency. This unique characteristic results in a different wavelength of wave propagation for each frequency. Thus, field survey methods that can propagate and record multi-frequency surface waves can be applied to characterise the elastic properties of the near surface. Surface wave energy sources range from vertically to horizontally orientated point sources and even through to background noise (Raines *et al.* 2011). Two thirds of the total seismic wave energy generated by a vertically orientated point source of pressure acting on a horizontal surface is in the form of Rayleigh waves, where the bulk of energy associated with Rayleigh waves is transmitted in the region within one wavelength of the surface (Richart *et al.* 1970). A large proportion of transverse wave phases are propagated in

the direction perpendicular to the axis of a horizontally orientated source. These include Love Waves and shear waves that are continually and critically refracted (Abbiss 1981). Background 'noise' sources consist of ambient microtremors, which occur constantly as cultural and natural background noise. Within noise records, Rayleigh wave phases can be separated from other seismic arrivals using a slowness-frequency (p-f) transform (McMechan & Yedlin 1981 & Raines *et al.* 2011) of microtremor field records. These same methods can also be applied to the analysis of Love waves.

Field survey set-ups range from the use of dual geophones to whole geophone arrays to record the characteristics of propagating surface waves. The Continuous Surface Wave (CSW) technique utilises a series of finite duration oscillations, each at a single frequency that are swept over a range of frequencies (often from 5Hz to 100Hz); field set-up shown in Fig. 1a. The ground motion is recorded using a small number of geophones placed inline with the vibrator, (Fig. 1a). The phase differences between the signals from the geophones are used as a basis for calculating wavelength and field dispersion curves (Richart *et al.* 1970, Joh 1996, Foti 2000 and Menzies 2001). Seismic refraction surveys utilise a co-linear source and multi-geophone array to record the waves that have been refracted along ray paths due to the velocity contrasts within the ground (Palmer 1986, Lankston 1990). In the case of a simple layer over a half-space, there is a critical angle at which an incident wave strikes the sub-surface boundary that causes a refracted wave to propagate in the half-space parallel to the boundary and to leak wave energy, through the upper layer, to the surface to be recorded by the geophone array; field set-up shown in Fig. 1b. Multi-channel Analysis of Surface Waves (MASW) can be performed on the data gathered using the same receiver array configuration adopted in shallow seismic refraction and reflection surveying (Fig. 1b). The source offset and array length control the effective maximum depth of penetration of the survey (Park *et al.* 1999 & Okada 2003). MASW techniques often employ impulsive sources capable of providing a broad range of frequencies. Consequently,

data gathered in the time domain must be transformed into velocity-frequency (or wave number-frequency) space using appropriate algorithms. Again, velocity dispersion curves are created, but the MASW technique differs from the CSW in that the phase velocities are calculated from the time delays for the different frequency components of the source signal to propagate through the receiver array (McMechan & Yedlin 1981, Thorson & Claerbout 1985, Park *et al.* 1999 & Rucker 2003).

The aims of this study were to evaluate some surface wave based methods and their limitations with regard to aggregate variability and thickness determinations. We compared the results of field assessments of sand and gravel sequences using different surface wave survey approaches. The first, followed a seismic refraction approach, the second, a CSW survey methodology, and the third, adopted the MASW analysis techniques to the original refraction field set-up and gathered data. The one dimensional velocity-depth profiles produced from the CSW surveys were also compared to logs of cone penetration resistance produced via operation of an ultra-lightweight cone penetrometer. The 2D velocity profiles produced from the shear wave refraction surveys were compared to reflection sections produced from continuous radar reflection surveys undertaken along the same line. An active extraction programme at the field site provided the opportunity to directly observe the subsurface geology during and after surveying and provide verification of all survey results.

Geology of the Study Area

Drift Geology

The study area was within the Tarmac Holme Pierrepont quarry, which was located approximately 5 km east of the city of Nottingham, UK (Fig. 2a). Shallow boreholes drilled in the vicinity of the site (within 500 m) sampled up to 6 m of poorly consolidated Holme Pierrepont Sand and Gravel (HPSG) overlying a bedrock sequence comprising consolidated mudstone and sandstone of Triassic age (Fig. 2b). The HPSG

typically comprises a sequence of poorly sorted gravels separated by medium-coarse grained sub-horizontal sand layers with locally developed cross stratification (Fig. 3a). Pebbles within the gravels are mostly rounded and < 50 mm in diameter, although individual pebbles > 100 mm have been recorded within the sequence (Fig. 3b). Locally, the long axes of the pebbles show a preferred orientation, imparting a pronounced fabric to the strata. At the Tarmac quarry the HPSG forms a series of tabular and lenticular bodies interpreted as low-profile bars that formed within a braided river system subject to seasonally high discharges of glacial melt water. Locally truncated ice wedge casts support the idea that the sediments were deposited in a periglacial environment on the margins of the Late Devensian ice sheet.

Solid Geology

The Gunthorpe Formation of the Mercia Mudstone Group forms the solid geology. Cuttings at the site revealed this to comprise interlayered red-brown and grey-green mudstone, siltstone and very fine-grained sandstone. Numerous, tough, dolomitic siltstone and fine-grained sandstone beds, (called 'skerries' by Charsley *et al.* 1990) commonly form upstanding features. The top surface of the exposed Mercia Mudstone at the trial site had a hummocky nature with depth of between 0.5m to 1m between the peaks and troughs (Fig. 4a). Often, the peaks were observed to coincide with the presence, at the surface, of more resistant dark grey-green siltstone bands of between 50mm to 200mm thick (Fig. 4b). Occasional gypsum (satin spar) bands of approximately 50mm thick were found at the trial site. In many locations over the trial site, the upper 1 m of the Mercia Mudstone was observed to comprise soft red-brown clays with 50 mm to 200 mm thick bands of broken up, grey-green siltstone (Fig. 4b). Below this were stiff red-brown clays and mudstones also containing grey-green siltstone bands (Fig. 4b).

Survey Planning: Initial Estimate of Properties

A key element of a sand and gravel thickness survey was the identification of the interface between the sand and gravel and the underlying bedrock. Survey quality would be improved with increased geophysical homogeneity within the sand and gravel and increased contrast between the geophysical properties of the sand and gravel and the underlying bedrock. A simplistic model can be represented by a layer of unconsolidated sediment of finite thickness overlying bedrock half space. Table 1 provides an initial estimate of the seismic properties of the drift and bedrock materials at site and the following discussion relates the initial rationale for studying aggregate heterogeneity and thickness. Generally, coarse sand and gravel deposits are well draining; water saturation can range from dry to fully saturated and is dependent upon a site-specific groundwater regime. A water table level within an upper layer would provide a boundary between significantly contrasting pressure wave velocities, whereas the shear wave velocities remain unchanged (Table 1). Also, the pressure wave velocity contrast between unconsolidated deposits and the underlying bedrock significantly reduces in the fully saturated case, whereas the equivalent shear wave velocity contrast remains unchanged with saturation. Interpretation of pressure wave surveys is often complicated by an apparent added layer due to water table levels within the top layer, which is not present in shear wave based surveys.

The values used in Table 1 were chosen on the basis of reviewing information on properties measured at other sites where similar materials exist. A key source of information for properties on the Gunthorpe Formation of the Mercia Mudstone was Forster (1992) and for the Holme Pierrepont Sand and Gravel were Butcher & Powell (1996) and Hight *et al.* (1997). Borehole SK63NW60 was within 100 m of the trial site (Fig. 2b) and revealed sand and gravel to a depth of approximately 5 m overlying mudstone of the Gunthorpe Formation. Survey design also benefitted from observations around the periphery of the survey areas of sections in the HPSG and of the upper

surface of the Gunthorpe Formation (about the 2.5 m Bench in Fig. 5a). On the basis of the estimated property values and aggregate thicknesses, the field surveys were configured only to investigate the top 10 m of the sub-surface.

Layout and Field Set-up of Surveys

Survey Orientations and Layouts

The surveys were undertaken in June 2003 during a programme of active extraction. Top soils were removed to 0.3 m depth and the aggregates were unsaturated due to continuous pumping to mitigate risk of running sands. Two 24 m by 48 m survey grids were established; one with the long axis orientated from east to west (denoted as increasing y) over an area where approximately a 2.5 m thickness of aggregate had been removed leaving a remaining aggregate thickness of 2.5 m (labeled the 2.5 m Bench in Figs. 5a, b); another with the long axis orientated from south to north over an approximate aggregate thickness of 5 m, (5 m Bench in Figs. 5a, c). The survey grids were established to evaluate the effectiveness of a range of geophysical methods in characterizing the aggregate sequence. Changes in elevation across the benches was surveyed relative to a base station, which was located at approximately BNG 462500 338600 (Fig. 5a). The change in elevations across the 2.5 m Bench was less than 0.7 m and across the 5 m Bench was less than 0.6 m. Testing of electromagnetic and radar techniques was done by surveying along lines parallel to the long axis of each grid at 1m stations with line spacings of 6 m across the short axis of each grid. Testing of the surface wave surveys was only undertaken on a single line, which formed the line of the refraction survey and extended across the long axis of the 5 m Bench as shown in Figs. 5a, c. Surface wave surveys were also undertaken on a line across the long axis of the 2.5 m Bench, which formed the line of a further refraction survey, but these were also supplemented with a further series of CSW surveys and dynamic cone penetration tests on a parallel line extending along another long axis of the grid offset by 6 m. Continuous surface wave (CSW) surveys at five locations along the lines of the shear

wave refraction surveys were undertaken on both the 2.5 m Bench and the 5 m Bench. The CSW surveys were spaced at 12 m apart and were positioned such that a CSW profile was coincident with the beginning, middle and end of the refraction lines.

The lightweight dynamic penetrometer was also deployed to depths of 3 m at positions 6 m to the south of the line of the refraction survey on the 2.5 m Bench. This equipment provided a depth profile of the dynamic cone penetration resistance calculated using the Dutch formula (Langton 1999). The tool was deployed offline so that the cone penetration resistance profile could be related to the geology in the vertical section immediately south of the refraction survey line on the 2.5 m Bench. Further CSW surveys (labelled CSW8 and CSW9 in Fig. 5b) were also undertaken at the two penetrometer locations.

Field measurements were validated with further post-survey observations of vertical sections through the aggregates to the bedrock a few metres offline from the refraction surveys. The results of the surface wave surveys were compared to observations of the vertical sections and the extensive suite of ground penetrating radar measurements gathered across the survey grids. The radar measurements were presented as radargram profile sections produced via continuous reflection profiling with a Pulse Ekko IV system (Sensors and Software Inc.) at 50 MHz and 100 MHz over the 5 m and 2.5 m Benches respectively. Section observations made during the return visits included a section that was close to the line of the refraction survey along the 2.5 m Bench, and also a section that ran parallel to the line of the refraction survey along the 5 m Bench. While this latter section was offset from the line of the refraction survey, the interpretation still benefitted from the comparison of the visual observation and the radar profile.

Refraction Survey Set-up

Following Abbiss (1981), a horizontally polarised seismic source was provided via imparting forcible translation into the ground along the long axis of a sleeper. A field vehicle provided a substantial downward force through the sleeper into the ground, and large pendulum hammers impacting on either side of the sleeper provided lateral translation. While some pressure wave disturbance is produced by this source much polarised transverse energy is produced that contributes to the generation of horizontally polarised shear body waves and surface Love waves (Abbiss 1981). Following the method described by Abbiss (1981) and Lankston (1990), the strong bi-polarity feature was exploited to preferentially stack shear wave energy to improve the shear wave to pressure wave signal ratio. This source produced measureable energy levels within a frequency band from 10 Hz to 75 Hz, but with peak energy around 30 Hz. Shot point spacing was chosen such that two midline and end line shots could be achieved. At each end, two offline shot positions were used at distances equivalent to one and two shot spacing increments beyond the end of the line. This equated to an 8 m spacing with 8 m and 16 m offline shots for the 2.5 m Bench and a 16 m spacing with 16 m and 32 m offline shots for the 5 m Bench. Geophones sensitive to horizontal motion were placed into the ground on a double spike. They were levelled and orientated to respond to the cross-line transverse displacement caused by horizontally polarised transverse waves propagated along the axis of the survey line. Geophone spacing was selected such that the direct and refracted arrivals could be distinguished on the end-line and mid-line field records. Geophone spacing was 1 m over the 2.5 m Bench and 2 m over the 5 m Bench. Field records were gathered on 24 geophones for each refraction survey using a Mark 3 ABEM Terraloc. Field records comprised 1000 data points gathered over 200 ms and 500 ms on the 2.5 m and 5 m Benches respectively. A means of triggering the seismograph system was provided by a piezoelectric pressure sensor that was attached to the railway sleeper.

Continuous Surface Wave Survey Set-up

The Continuous Surface Wave (CSW) technique used a vertically polarised electromagnetic vibrator to introduce a multi-frequency sweep (in the range 5-100 Hz) into the subsurface. The source was set to vibrate over a series of discrete frequencies and placed on the ground surface 1 m away from the nearest geophone for the 2.5 m Bench (2 m for the 5 m Bench) of an array of 5 geophones, spaced at 1 m for the 2.5 m Bench (2 m for the 5 m Bench). The phase shift was measured between the geophones and used to calculate the wavelength and phase velocity of the Rayleigh wave following methods by Richart *et al.* (1970), Joh (1996), Foti (2000) and Menzies (2001). Field velocity measurements are made over a range of frequencies to generate a dispersion curve, which can be inverted to produce a velocity-depth profile for the shallow subsurface (Joh 1996 and Foti 2000). The frequencies propagated and the distance between the nearest and farthest receivers in the array generally sets the depth range of investigation. Joh (1996) suggested wavelengths as short as one third the shortest receiver spacing, 0.35 m (2.5 m Bench) or 0.7 m (5 m Bench) and as long as three times the largest receiver spacing, 12 m or 24 m in this case could be measured. While using this set up, field data have to be inspected to ensure that the phase measurements made at the shorter wavelengths take full account of the complete number of wavelength cycles that are propagated between neighbouring receivers to avoid erroneous measurements caused by phase wrapping leading to an underestimation of phase by two Pi radians (Joh 1996, Park *et al.* 1999 & Foti 2000). The range of wavelengths propagated is given by the ratio of the phase velocity to the frequency and was anticipated to be from 1 m (minimum velocity 100 ms^{-1} at maximum frequency 100 Hz) to 40 m (maximum velocity 200 ms^{-1} at minimum frequency 5 Hz).

The dispersion curve is interactively forward-modelled to determine the subsurface shear-wave velocity profile (Joh 1996, Foti 2000 & Raines *et al.* 2011). The solutions provided are non-unique (i.e. more than one profile model can produce the same

dispersion curve) and for this reason, inversion techniques use a first tentative profile of the site and adjust it by comparing the results of the numerical simulation to the dispersion curve obtained from the field test (Tokimatsu *et al.* 1992 & Yuan & Nazarian 1993). The simplest method is attribution of a factored shear wave phase-velocity (usually 0.9 times Rayleigh wave velocity Joh 1996, Foti 2000 & Okada 2003) to a depth equivalent to a fraction of the Rayleigh wavelength, λ. Fractional depth factors range from $\lambda/4$ to $\lambda/2$ (Jones 1958, Ballard & McLean 1975 & Abbis 1981). Gazetas (1982) recommended that $\lambda/4$ be used where the stiffness increases significantly with depth and that $\lambda/2$ is used for more homogeneous stiffness profiles. However, a factor of $\lambda/3$ is most commonly used (Bullen 1963 & Richart *et al.* 1970) because a significant proportion of the particle motion in the ground associated with Rayleigh wave propagation is approximately at this depth (Fig. 6a). The particle displacement has a non-monotonic profile for both the vertical and the horizontal components of the Rayleigh wave. A significant proportion of displacement is between the interval 0.2 to 0.4 times the wavelength, whereas, particle displacement for the Love wave reduces exponentially with depth (Fig. 6b). Thus, for Love waves, which is a transverse surface wave that propagates at the same velocity as a shear wave, nearer surface properties can have a more significant effect upon phase velocity. It becomes more difficult to satisfactorily select a depth of investigation for Love wave at which the velocity can be attributed, which is discussed below. More computationally involved inversion includes the production of a state vector describing the interface properties between each layer in the model, which are defined by a transfer matrix. Propagation matrices are also determined, which describe how the seismic waves are transmitted through the layered model. Each of the transfer matrices is converted into a series of equivalent stiffness matrices, which are combined into a global stiffness matrix for the complete soil profile, from which a theoretical dispersion curve is calculated. The detail of the inversion is beyond the scope of this paper, but thorough descriptions can be found in

Thomson (1950), Haskell (1953) and Kausel & Roesset (1981). Available inversion software includes SURF by Herrmann (1998) and WinSASW by Joh (1996; 2002).

Phase velocity-depth profiles of up to 10 m were produced using the simple inversion based upon the factored wavelength. Some of the field data were further inverted to produce shear wave velocity profiles with depth using WinSASW 2.2.1 following the procedure described by Joh (1996). The inversion is non-unique and the ground properties from observations of vertical sections, or, as characterised by the cone penetration resistance profiles, were used to aid the procedure, where these were available.

Additional MASW Processing of Refraction Records

Some of the field traces gathered during the refraction survey were transformed into the phase velocity-frequency domain using a procedure based upon the methods described by McMechan & Yedlin (1981), Horike, M. (1985), Louie (2001) and Raines *et al.* (2011). The time delay between a signal on the wiggle trace of the first geophone (nearest to source) and equivalent signals on the successive traces within the whole field record, such as Fig. 7a was used with the spacing between the geophones to calculate a delay velocity as illustrated in Fig. 7. The process includes the application of the Fourier transform to decompose the propagating disturbance into a band of frequencies. The velocity calculation made on each frequency component provides the phase velocity, or the velocity at which each frequency component moves through the geophone array (Fig. 7b). The basis of the phase velocity-frequency transformation is the “slantstack” described by Thorson & Claerbout (1985) and it is also described in more detail by Pullammanappallil *et al*. (2003). The velocity-frequency transformation also produces an indication of the distribution of the spectral energy across a range of velocities at each frequency. With the field data transformed and plotted against these axes, surface wave propagation modes, such as Rayleigh and Love waves are picked out as the packets of peak energy at low velocities along the frequency axis (Fig. 7b),

described by Pullammanappallil *et al*. (2003) as picking 'along the envelope with the lowest phase velocities'. Low energy also appears to be smeared at high velocities decreasing from 1000 ms^{-1} at 70 Hz to around 600 ms^{-1} at 95 Hz. This is attributed by many authors to higher order surface waves (Park *et al.* 1999, Louie 2001, Pullammanappallil *et al*. 2003, Rucker 2003 & Okada 2003). The dispersion curve, such as in Fig. 7c is created by running a peak detection algorithm over the spectral energy plotted against each frequency, shown by the green crosses on Fig 7b. Pullammanappallil *et al*. (2003) also describe picking where a 'slope feature' across the frequencies defines the lowest phase velocity curve, but if the incorrect 'slope feature' is selected, this can lead to inaccurate velocity attribution at depth. To demonstrate the potential problems of incorrectly picking sloping features, which can happen with noisy data, the lower and upper velocity bounds associated with each central peak energy are also plotted on Fig. 7b. The velocity range between the upper and lower bounds increases at lower frequencies. This smearing of energy is proportional to the changes in wavelength and leads to increasing inaccuracies in the ground velocity attribution at greater depths, for example, if these bounds are used. Traces from all geophones in the array and also gathers comprising traces from groups of six geophones centred on the CSW experiments were used to compute the dispersion curves presented in this paper. In each case, a group of three dispersion curves was provided via picks along the peak spectral energy and along the upper and lower boundaries. This was done to provide a comparison of the velocity depth profiles produced by the CSW and MASW techniques, and also, as a means of indicating the potential range of velocity attribution if incorrect slope features are used. Ground velocity attribution is also affected by the wavelength factors used to determine the depth at which the phase velocity is ascribed. The geophones were sensitive to horizontal displacements, thus the dispersion curve picked using the peak spectral energy will represent the phase velocity of a Love wave propagational mode. Unlike Rayleigh waves which have peak particle displacements

between depths 0.2 – 0.4 times the wavelength, Loves wave displacements decrease exponentially with depth (see Fig. 6). In the discussion below we also consider the effect of wavelength factors. Other sources of error include velocity overestimation from surface waves propagation directions oblique to the geophone array (Louie 2001 & Rucker 2003). However, this was avoided in our case by use of inline shots ensuring wave propagation parallel to the geophone array.

Survey Data and Resulting Interpretations

Refraction Surveys

The field data were generally of good quality (Fig. 8a) enabling identification of direct and refracted events, and development of a time-distance plots from first break picking (Fig. 8b). The curvature on the direct arrival was a result of the continuous refraction of the shear wave due to the shear wave velocity increasing with depth, which is described by Abbiss (1981). The time-distance plot of the survey over the 2.5 m Bench was organised into the simple model of a single, finite thickness low velocity layer of mean velocity of 214 ms^{-1} overlying a higher velocity bedrock of mean velocity 972 ms^{-1}. This related to a mean layer thickness of 3.6 m to the top of the refracting horizon calculated along the time-distance plot, where the standard deviation along the calculation was 0.5 m. The interface between the base of the HPSG and the top of the Gunthorpe Formation was at approximately 2.8 m depth. This did not form the main critical refractor, which was possibly a deeper horizon within the bedrock. The time-distance plot of the survey over the 5 m Bench was organised into a three layer model of two finite-thickness layers overlying a higher velocity halfspace, as shown in Table 2. The mean velocity in Layer 1 (topmost) was 185 ms^{-1}, in Layer 2 (middle) was 420 ms^{-1} and in the underlying halfspace was 1283 ms^{-1}. This related to mean thicknesses of 3.2 m with a standard deviation of 1.2 m for Layer 1, and 7.6 m with a standard deviation of 0.85 m for Layer 2. The interface between the base of the HPSG and the top of the Gunthorpe Formation was at approximately 5 m depth; but velocity contrasts within the

HPSG and the Gunthorpe Formation were the cause of refracting horizons at the bases of Layers 1 and 2. The actual refraction may also be complex as indicated by great variability within the layer velocities determined from the various shot points for both forward and reverse directions.

Data from the time-distance plots were further processed involving phantoming, velocity analysis and depth migration following procedures described by Palmer (1986). On the 2.5 m Bench, reciprocal times for the refracting horizon were 62.1 ms to the west and 61.6 ms to the east. Depth migration using the average velocity method provided a depth range from 3.6 m to 3.8 m for the refracting horizon, shown in Fig. 9a. Along the refraction profile, the relief of the bedrock top-surface was observed to be hummocky, ranging from 2.3 m deep to 2.8 m deep, as shown in Fig. 9b. Fig. 9a. shows the refracting horizon (yellow) plotted at the equivalent lateral and vertical (depth) scale and overlain onto a ground penetrating radar section. Because the sand and gravel were desaturated by pumping, the dielectric properties of the Gunthorpe Formation contrast strongly with the HPSG. Thus, the base of the HPSG was well defined on the radargrams with a strong reflector from which the horizon was interpreted.

On the 5 m Bench, reciprocal times for the refracting horizon were 110.2 ms in the forward direction and 109.3 ms in the reverse directions. Depth migration using the average velocity method provided a depth range from 2.5 m to 5.2 m for the refracting horizon between Layer 1 and Layer 2 and a range of 16.5 m to 16.9 m for the base of Layer 2. Fig. 10a shows the shallower refracting horizon with respect to the interpreted top-surface of the bedrock on the radar section. This shallow refraction horizon follows a strong reflector on the radar section that dips southwards from Y = 30 m to station Y = 8 m. A similar feature was observed on the radargram along parallel profile situated 6 m to the east, Fig. 10b, which was observed in the vertical section to coincide with a unit of weakly cemented very gravelly coarse sand. Where it was excavated,

immediately above the bedrock, this unit was at least 1 m thick. Cementation was provided by orange-red, ferruginous iron oxide and black manganese dioxide (pyrolusite) cements, enabling a vertical section to be cut in the unit, which was tough to dig. It was considered that the cementation caused increased stiffness and shear wave velocities within this unit. Thus, the velocity profile through the aggregates is not likely to be normally dispersive, i.e. have a monotonic velocity increase with depth. For example, some units within the sand and gravel would exhibit increased shear wave velocities because of the increases in stiffness associated with weak cementation or increased density due to poor sorting. Given the depositional regime, these would provide laterally discontinuous, shallow horizons that would refract energy differently from shot points depending upon the relative offset between the shot and the stiffer units. This causes much lateral heterogeneity in the velocity structure within the sand and gravel, which contributes to great variability in the layer thickness calculations using refraction methods. A variable velocity structure within both the HPSG and the underlying bedrock also reduces the effectiveness of the refraction method to characterise the drift. The following interpretations based upon the CSW and MASW methods provide further confirmation of very poor velocity contrasts, indicating that shear wave refraction methods would generally be ineffective when characterising aggregate thickness.

Continuous Surface Wave Surveys

A total of thirteen CSW surveys were undertaken over the site, comprising seven over the 2.5 m Bench, five over the 5 m Bench and one over the bedrock mudstone of the Gunthorpe Formation. Field shear wave velocities were derived via a multiplication of the field Rayleigh wave velocity by a factor of 1.1 and plotted against a depth equivalent to one-third of the wavelength. Generally, the maximum penetration depths of surveys on sand and gravel deposits were from 6m to 12m below the surface. The

field data quality was generally very good but phase measurement errors were encountered especially at higher frequencies. These errors were caused for example, by ambiguities due to incorrect counting of wavelengths and by noise interference affecting the phase measurement (Fig. 11). On tests on the 2.5 m Bench it was difficult to distinguish high velocity units on velocity-depth profiles created from the simple 1/3 factored wavelength inversion of the dispersion curve. Some profiles, such as CSW10 in Fig. 12, exhibited minor purturbations at depths that coincided with high velocity layers in the profiles inverted using the state vector method. For example, minor purturbations on profile CSW10 between 1.25 m and 1.5 m depths coincided with a higher velocity layer overlying a lower velocity layer at 1.5 m depth. The high velocity layers appear be associated with matrix-supported coarse gravel lenses within the sequence, where velocities were over 175ms^{-1} on CSW10 and over 200 ms^{-1} on CSW9 where the gravel unit was observed in a vertical section. Very high cone penetration resistances are recorded in these lenses as the tip of penetrometer bore against a large pebble until it eventually fractured or was pushed to the side. This produced a characteristic signature on the penetration profile of a series of very high resistance peaks within small depth intervals, for example, the interval from 1.1m to 1.5m below the surface at CSW9. It was suspected that a either a continuation of the same gravel lens or a related unit was the cause of the high velocity interval between 1 m and 1.5 m on the inverted CSW10 profile.

The top bedrock was observed to be approximately 2.2 m below the ground surface on CSW9 (undertaken next to the vertical section) and interpreted to be at a similar level on CSW10 (Fig. 12). At CSW9 (X=0, Y=12), it is characterised by ‘step-like’ increase on the penetration resistance profile. At this location, the bedrock top surface was observed to be hummocky with the crest of a small ridge, consistent with the bedrock having relatively high penetration resistance, characteristic of a more competent mudstone and possibly siltstone bands. The upper 0.5 m interval of the bedrock was

characterised by penetration resistances generally below 10 MPa, whereas resistances greater than 20 MPa occur beyond 2.6 m depth. This boundary closely coincided with a step-wise increase in velocity with depth at CSW9 on the inverted velocity profile, where the velocity of the upper weathered zone is around 185ms^{-1}, increasing to above 300ms^{-1} in the zone below. Note however, the very low contrast between the shear wave velocities of the upper, weathered zone of the Gunthorpe Formation and the base of the sand and gravels (around 160 ms^{-1}). This velocity profile is highly consistent with the refraction survey, e.g. where the potential refracting horizon at 2.6 m deep is caused by a hard, competent unit within the bedrock with a shear wave velocity approximately twice as fast as the velocity through the soil and weathered bedrock above.

The near surface shear wave velocity profiles of the exposed Gunthorpe Formation inverted using the simple factored wavelength and the state vector methods are plotted against the cone penetration resistance profile in Fig. 13. The top of the exposed mudstone bedrock is characterised by a 1 m thick low velocity interval with inverted velocities between 88 and 102 ms^{-1}. Penetrometer measurements at the same location also show low cone resistance values (below 3 MPa) in the upper 1 m. It is considered that the top of the bedrock exhibits lower penetration resistances and lower velocities when the overburden from the HPSG is removed. Vertical sections through the top of the Gunthorpe Formation revealed soft grey and red-brown clay with bands of grey-green siltsone and red-brown mudstone to a depth of about 1 m, overlying more competent, stiff red-brown mudstone (see Fig. 4b). Interestingly, in many of the bands, the siltstone was broken up into roughly cubic blocks or around 30 – 50 mm in size, as though some process had caused the bands to shatter. (The authors have observed similar shattering effects in south Nottinghamshire Blue Anchor siltstones when removed from the formation and used as fill.) The upper 1 m of the Gunthorpe Formation was considered to be a weathered zone with characteristics of low

penetration strength and low shear wave velocity; the shear wave velocity within this zone being so low that it would not provide the contrast required to create the critically refracted ray path in the refraction survey. It was considered that the weathering profile would have developed prior to the deposition of the HPSG. Both cone penetration resistance and the inverted shear wave velocities showed significant increases below 1 m. This is consistent with the observations from exposed sections of the upper profile in the Gunthorpe Formation, and also with the refraction survey indicating that higher velocity refractors would be within the deeper, unweathered bedrock.

Observations from a vertical section through the 5 m Bench, 6 m offline from the CSW surveys revealed intervals of cemented coarse gravelly, sands and sandy gravels. Sequences of note included a red-brown gravel, a red-brown gravelly coarse sand and a buff sandy gravel within the interval from 1.2 m to 2.7 m, and also, the basal gravel of 1 m thickness resting immediately on the top of the Gunthorpe Formation, within which vertically cut faces were completely self supporting. Such units were the likely cause of the shear wave refraction along higher velocity, vertically and laterally discontinuous, shallow horizons within the aggregates causing bending of the wave front back towards the surface. These can be lenticular units over a narrow depth interval, as seen between 1 – 1.5 m in Figs. 14a and b, where they cause an increase in the velocity-depth gradient on the field data and are inverted as a fast layer (with a velocity of 193ms^{-1} in CSW5). They also appear at greater depths as thicker sequences, where the top sequence is marked as a step-wise increase in the velocity profile inverted using the state vector method, e.g. up to 190ms^{-1} at 2 m in CSW3 and up to 207ms^{-1} at 3 m in CSW5. These mark the tops of intervals of relatively high velocities (generally >200ms^{-1}), which in both cases, extends into the underlying bedrock. Hence, the top of these sequences and not the top of the bedrock provide the velocity contrast to the HPSG above, along which there would be significant refraction leading to the return of much wave energy to the surface.

MASW Processing of Refraction Survey Field Records

Refracted body waves appear to increase in velocity with shot-receiver distance on the field records. MASW processing of the offline shots during the shear wave refraction survey show how this mode plots in the velocity frequency space. Fig. 15a shows an example of a 24 channel offline shot record from the refraction survey over the 5 m Bench. The horizontally polarised source generated: Love waves, seen on the field record as low velocity mode from 0.25 to 0.5 s across the array, a critically refracted head shear wave, highest velocity mode from 0.09 to 1.2 s (but note how the slope changes suggesting a laterally variable velocity, e.g. as recorded in Table 2) and continuously refracted body shear waves that appear to leak from the Love wavefront along faster pathways, including along shallow, near-surface refractors (see also Fig. 1b).

A significant proportion of the refracted energy is not in the form of a critically refracted head wave, but, because of the heterogeneity of the velocity section through the HPSG, it contributes to the continuous refraction of body shear waves (Fig. 15a). While the HPSG has a heterogeneous velocity structure including discontinuous, shallow refractors, effective stress effects cause the overall ground velocity to increase with depth (Gunn *et al.* 2003). This velocity structure causes the body waves to continually refract back towards the surface (Abbiss 1981). The Love wave propagates along the surface and body shear waves penetrate into the ground at a range of angles to the ground's surface (see Fig 1b). Generally, the shallow angle body waves are more likely to travel along shallower, lower velocity pathways and return to the surface after a shorter travel path than the wider angle body waves (Abbis 1981 & Foti 2000). The shallow angle body waves may contain a greater proportion of higher frequencies due to less attenuation over shorter travel paths but this depends upon the pathway properties. On the velocity-frequency space, critically and continuously refracted body waves mainly plot around 25 – 35 Hz, i.e. the central frequency band produced by the source,

with a velocity range from around 300 ms^{-1} at the higher frequencies to 600 ms^{-1} at the lower frequencies, i.e. the velocity range of the layer 2 refractors identified in Table 2. Some higher mode surface waves also plot within this range of velocities either around 30 Hz or at higher frequencies (Fig. 15a). The higher velocity, refracted propagation modes generated by a horizontally polarised source can be removed by selective filtering in the velocity-frequency space, called f-k filtering or dip filtering, which is routinely used in seismic processing, REFs. Fig. 15b shows the resulting field record with a significant proportion of the refracted body waves removed leaving the surface wave. Artefacts of the filtering include the apparent increase in the phase velocities over the higher frequencies from 45 to 60 Hz. While the filtering simplifies the velocity-frequency plot and aides distinguishing the differing propagation modes, such higher frequency artefacts are not significant in the unfiltered record from which a more representative dispersion curve can be picked from the peak energy. The Rayleigh wave dispersion curve from CSW3 is also plotted (open squares) on Fig. 15b for comparison with the Love wave. The Love wave appears as a weakly dispersive mode in the velocity-frequency space, but note that it still suffers with the low frequency smear discussed above. The different particle displacement characteristics, and in part, differences in the whole propagation pathways contribute to the observed differences between the Rayleigh and the Love wave dispersion curves.

In Fig. 15, the source of the Rayleigh wave gathered from CSW3 was near the array, while the source of the Love wave was approximately 50 m away. The Love wave propagation recorded during the refraction survey on geophones localised about the zone where CSW3 was also recorded contain a similar overall phase velocity character to the Rayleigh wave gathered by CSW3. But, ‘far offset’ effects as described by Park et al. (1999) were suspected on the field seismograms recorded by the geophones at the end of the array furthest from the source. Park *et al.* (1999) attributed this effect to a lowering of the higher frequency energy content of the surface wave with an associated,

apparent, relative increase in the high frequency content of faster, body waves. These effects are characterised by velocity measurements at higher frequencies relating to body waves and not surface waves (Park et al. 1999), and because the body waves have propagated via deeper pathways, they tend to be of greater velocity than the surface waves. They can be observed by MASW processing the field seismograms gathered on a small sub-group of geophones, in this case, centred about the location where the CSW tests were undertaken. Frequency – velocity transformations were calculated using 6-channel gathers of channels 3 – 8, 9 – 15 and 15 – 20 centred on profiles CSW2, CSW3 and CSW4 respectively (see Fig. 5c). Dispersion curves were picked along the peak energy, upper and lower boundaries and compared to dispersion curves derived from the respective CSW measurements, Fig. 16.

Overall, the Love wave dispersion curves picked along the peak energy provide higher phase velocity characteristics than the Rayleigh wave dispersion curves. This is consistent with the Love wave, which is equivalent to the horizontally polarised shear wave having a higher propagation velocity than the Rayleigh wave. Body wave contamination can be observed at higher frequencies on the velocity-frequency plots, with refracted events contributing to the energy centred around 30 Hz. 'Far offset' effects on channels 15-20, furthest away from the source are suspected to contribute to the increasing difference between the higher frequency phase velocities determined by the CSW and Love wave dispersion curves (Fig 16c). Fig. 17 shows the Love wave phase velocities for each dispersion curve in Fig. 16 plotted at a depth equivalent to one half and one third the wavelength. For comparison, the velocity-depth profiles determined from the CSW surveys undertaken at the same location are also plotted at a depth equivalent to one third wavelength (where shear wave velocity factored at 1.1 times Rayleigh velocity was plotted for the CSW). The upper / lower bounds of the spectral energy packet provide an indication of the potential velocity over / under estimation, if for example, slope features are inappropriately used with MASW

approaches. If the data suffer low frequency smear, the velocity range between the upper and lower bounds can be over 100 ms^{-1}, for example at 7 m depth in Fig. 17b. CSW 2 and 3 are non-normally dispersive sequencies, and the CSW velocity-profiles show similar overall velocity structure to the ½ wavelength Love wave profiles at shallow depths above approximately 5 m depth, where the CSW and the ½ wavelength central (peak spectral energy) profiles correspond well in the interval above a high velocity layer between 3 and 4 m in these sequences that was coincident with a cemented coarse, sandy gravel – see Figs. 10b, 17a, b. The same depth forms the upper boundary of a thicker interval of higher velocities at CSW4, where there is improved correspondence between CSW4 and the Love wave peak spectral energy profile below 4 m depth, Fig. 17c. The non-normally dispersive velocity profiles of CSW2 and CSW3 raise some interesting issues regarding the differences between the techniques of CSW using Rayleigh waves and the MASW using horizontally polarized Love waves. On the two nearest groups of geophones (Figs. 17a,b), the ½ wavelength Love Wave inversion provide a better comparison with associated CSW 2 and 3 for the higher frequency, shallower depth information. Whereas, on the farthest geophone group (Fig. 17c), the 1/3 wavelength Love Wave inversion provides a better comparison for the low frequency, deeper information. The CSW profiles contain far greater information relating to the heterogeneity in the velocity structure in the HPSG (above 5 m depth) and the bedrock below. In particular, the CSW profiles contain more high frequency, shallow depth information relating to the velocity profile in the top 1 m. In part, this is related to the frequency characteristics of the sources, i.e. the horizontally polarized source has a peak frequency around 30 Hz whereas, the CSW source specifically produces frequencies up to 100 Hz. Also, the large source-receiver distances (50 m) used in the Love wave survey leads to loss of information due to attenuation with distance affecting the higher more than the lower frequencies. This will serve to compound ‘far offset’ problems associated with erroneously high velocity estimation at

high frequencies and may contribute to the large velocity contrast between the Love wave and CSW surveys in Fig. 17c. Overall, where body waves don't contaminate the surface wave dispersion curves plotting the Love wave velocities at a depth equivalent to ½ wavelength provides better correspondence to the velocity profile created from the factored Rayleigh waves plotted at a depth equivalent to 1/3 wavelength from the CSW surveys.

Conclusions

Surface waves are dispersive and can be used to investigate the shear wave velocity-depth profile of the ground. Surface wave surveys require a field source and receiver array, which differ in their configuration depending upon whether Love or Rayleigh wave surveys are undertaken. To enable recording of coherent surface waves and correct velocity attribution, field procedures should ensure that wave propagation is parallel to the receiver array. The Love wave travels at the same velocity as a shear wave but the Rayleigh wave has a lower velocity. The particle displacement characteristics within the ground are very different for Love wave and Rayleigh wave propagation. Simple shear wave velocity-depth inversion is achieved by attribution of an appropriately factored shear wave velocity at an appropriate depth of investigation in relation to how the particle displacement characteristics change with depth relative to the wavelength of the surface wave. Rigorous inversions involve iterating an initial ground model, usually based upon a simple factored wavelength velocity-depth profile. Because the solutions are non-unique, further relevant data can be used to constrain the modelled profiles, for example cone penetration resistance profiles to aid the relative layer velocities.

The near-surface conditions of glaciofluvial sand and gravel deposits have been shown to be highly heterogeneous. Controlled by the depositional processes and the materials, the scales of observed heterogeneity ranged from approximately metric as in bedding, to

centimetric of some of the fluvial structures. Surface wave survey methods can be applied and interpreted to characterize the metric scale of heterogeneity, such as bedding. Reliable assessment of the aggregate sequence thickness was largely unsuccessful with all the methods, due mainly to the very poor velocity contrast at the interface between the base of the aggregates and the top bedrock, which comprised weak and weathered rock. Wetting fronts due to a fluctuating water table have deposited films of iron (red) and manganese (black) oxide particularly within the coarser, higher permeability materials, which provide weak cementation to parts of the sequence. Observations of these cemented gravel beds coincided with high velocity layers within the aggregate sequence, and thus the soil profiles were invariably not normally dispersive.

The use of standard refraction approaches provided particularly poor results. Near surface, cemented fast layers presented shallow refracting horizons and contributed to an underestimation of aggregate thickness using refraction methods with a horizontally polarised shear wave source. Much more detailed inversion of the velocity-depth profiles was provide from simple, factored wavelength inversions derived using CSW and MASW methods. These approaches, especially the CSW, enabled the identification of the non-normally dispersive velocity structure within the HPSG. In these field trials, the CSW profiles contained more detailed information relating to the velocity structure than the MASW. This was due to the relatively greater levels of the high frequency energy made available from a smaller source-receiver distance limiting attenuation and the high frequency capability of the source. In the case of large source-receiver distances, such as over 50 m body wave contamination can cause erroneously high velocity attribution, especially to the high frequencies with the MASW approach. Also, incorrect velocity attribution can occur with MASW processing by picking slope features related to the upper or lower energy bounds of the surface wave on the velocity-frequency plot, which should be avoided as it can lead to significant velocity

over or under estimation. Close correspondence existed between shear wave velocity-depth profiles picked using a one third wavelength Rayleigh wave from the CSW survey and a one half wavelength from the MASW processing of Love waves.

2D sections can be built up from a series of inline velocity-depth profiles spaced at a suitable interval to capture the structural heterogeneity at a suitable scale, which in this case would only be a few metres. These could be derived either using a series of CSW surveys of using a MASW approach with overlapping gathers of selected channels in sub-groups of six geophones from larger geophone arrays. Impulsive sources are more convenient and combined with spectral processing yield results far more rapidly than continuous frequency approaches such as used in CSW surveys. Thus, provided a source or sources can be used to generate a relatively wide frequency band, e.g. 5 – 100 Hz, a MASW survey will provide more effective ground coverage. Simple MASW survey field procedures to guard against 'far offset' effects include the use of a constant source-nearest receiver distance and roll along receiver array relocation to extend lateral coverage. While either Love or Rayleigh surface waves can be used with the MASW approach, because the most commonly available geophones respond to vertical ground motion, vertically orientated impulsive sources such as hammer on plate are more often deployed in Rayleigh wave surveys.

Acknowledgments

This paper is published with the permission of the Executive Direct of the British Geological Survey (NERC). The authors express their gratitude to Tarmac Ltd. For access to the Holme Pierrepont quarry.

References

Abbiss, C.P. (1981). Shear wave measurements of the elasticity of the ground. Geotechnique, 31, (1), pp91-104.

Ballard, R.F. & McLean, F.G. 1975. Seismic field methods for in situ moduli. Proc. Conf. on In Situ Measurement of Soil Properties. S*pec. Conf. Geotech. Eng. Div., A.S.C.E.*, Vol 1, pp121-150.

Bullen, K.E. (1963). An Introduction to the Theory of Seismology. Cambridge University Press, 390p.

Butcher, A.P. & Powell, J.J.M., (1996). Practical considerations for field geophysical techniques used to assess ground stiffness. Proc. Int. Conf. on Advances in Site Investigation Practice, London, Thomas Telford, pp.701-714

Charsley, T.J., Rathbone, P.A. and Lowe, D.J., (1990). Nottingham: A geological background for planning and development. BGS Technical Report WA/90/1.

Clayton, C.R.I. 1990. SPT Energy Transmission: Theory, Measurement, and Significance. *Ground Engineering*, v. 23:10, p. 35-43.

Forster, A. (1992). The engineering geology of the area around Nottingham. 1:50 000 Geological map sheet 126 (Nottingham). British Geological Technical Report No. WN/92/7.

Foti, S. (2000). Multistation methods for geotechnical characterisation using surface waves. Ph.D. Thesis, Politecnico di Torino. 229p.

Gazetas, G. 1982. Vibrational characteristics of soil deposits with variable velocity. *Int. Jour. Numerical and Analytical Methods in Geomech*., Vol 6, pp 1-20.

Gunn DA, Jackson, PD, Entwisle, DC, Armstrong, RW and Culshaw, MG, 2003. Predicting subgrade shear modulus from existing ground models. NDT&E Int. 36, (3), 135 – 144.

Gunn, D.A, Nelder, L.M., Chambers, J.E., Reeves, H., Freeborough, K., Jackson, P., Stirling, A.B. & Brough, M., (2005). Geophysical monitoring of the subgrade with examples from Leominster. Proc. 8th Int. Conf. Railway Engineering, London.

Gunn, D.A., L.M. Nelder, J.E. Chambers, M.R. Raines, H.J. Reeves, D. Boon, S. Pearson, E. Haslam, J. Carney, A.B. Stirling, G. Ghataora, M. Burrow, R.D. Tinsley, W.H. Tinsley, R. Tilden-Smith, (2006a). Assessment of railway embankment stiffness using continuous surface waves. Proc. 1st Int. Conf. Railway Foundations, Birmingham, September 2006, pp94-106.

Gunn, D.A., S.G. Pearson, J.E. Chambers, L.M. Nelder, J.R. Lee, D. Beamish and J.P. Busby, R.D. Tinsley & W.H. Tinsley. (2006b) An evaluation of combined geophysical and geotechnical methods to characterise beach thickness. Q.J.E.G.H. 39, 339-355.

Gunn, D.A, Reeves, H., Chambers, J.E., Pearson, S.G., Haslam, E., Raines, M.R., Tragheim, D., Ghataora, G., Burrow, M, Weston, P., Thomas, A., Lovell, J.M., Tilden Smith, R., Nelder, L.M., (2007). Assessment of embankment condition using combined geophysical and geotechnical surveys. Proc. 9th Int. Conf. Railway Engineering, London.

Haskell N.A. 1953. The dispersion of surface waves on multilayered media. Bull. Seismological Society of America, vol. 43, (1), pp 17-34.

Herrmann R. 1998. Computer programs in seismiology-manual. Univ. St. Louis, USA. www.eas.slu.edu

Hight, D.W., Bennell, J.D., Chana, B., Davis, P.D., Jardine, R.J. and Porovic, E. (1997). Wave velocity and stiffness measurements of Crag and Lower London Tertiaries at Sizewell Geotechnique, 47, (3), pp 451 – 474.

Horike, M. (1985). Inversion of phase velocity of long-period microtremors to the S wave-velocity structure down to the basement in urbanized areas, J. Phys. Earth, 33, 59-96.

Jackson, P.D. & McCann, D.M. 1997. Cross-hole seismic tomography for engineering site investigation. In: McCann D.M., Fenning P.J. & Reeves, G.M., editors. Modern geophysics in engineering geology. Geology Special Publication. London: Geological Society Engineering, p. 249–66.

Jackson, P.D., Gunn, D.A., Flint, R.C., McCann, M.C.,Bent, M. & Howes, D. 2001. Cross-hole seismic measurements for detection of disturbed ground beneath existing structures. *NDT & E Int.* (34), 2001, 155-162.

Joh, S.H. (1996). Advances in the data interpretation technique for spectral analysis of surface waves measurements. Ph.D. Thesis. University of Texas, USA. 240p.

Joh, S.-H. 2002. WinSASW Version 2.0. Data interpretation and analysis for SASW measurements. User's guide. Dept. Civil Engineering, Chung-Ang University, Korea.

Jones, R.B. 1958 In-situ measurement of the dynamic properties of soil by vibration methods. *Geotechnique*, vol. 8 (1), pp. 1-21.

Kausel E. & Roesset J.M. 1981. Stiffness matrices for layered soils. *Bull. Seismological Society of America*, vol. 71 (6), pp 1743-1761.

Langton, D.D., (1999). The Panda lightweight penetrometer for soil investigation and monitoring material compaction. *Ground Engineering*, September, pp 33 – 37.

Lankston, R.W., (1990). High-Resolution Refraction Seismic Data Acquisition and Interpretation. In: Ward, S.H., (Ed.), Geotechnical and Environmental Geophysics I: Society of Exploration Geophysics. pp 45-73.

Liao, S.S.C. and Whitman, R.V. 1986. Overburden Correction Factors for SPT in Sand: *Jour. Geotech. Eng., A.S.C.E.*, v. 112:3, p. 373-377.

Louie, J, N. 2001. Faster, Better: Shear-wave velocity to 100 meters depth from refraction microtremor arrays: Bu*lletin of the Seismological Society of America*, v. 91, p. 347-364.

Menzies, B.K. (2001) Near-surface site characterisation by ground stiffness profiling using surface wave geophysics. Instrumentation in Geotechnical Engineering. H.C.Verma Commemorative Volume. Eds. K.R. Saxena and V.M. Sharma. Oxford & IBH Publishing Co. Pvt. Ltd., New Delhi, Calcultta. pp 43-71.

McMechan, G. A., and Yedlin, M. J., 1981. Analysis of dispersive waves by wave field transformation, *Geophysics*, **46**, 869-874.

Murphy, J.R., Davies, A.H., Weaver, N.L., 1971. Amplification of seismic body waves by low velocity surface layers. Bull. Seismol. Soc. Am. 61 (1), 109– 145.

Okada, H. 2003. *The microtremor survey method*. Geophysical Monograph Series. No. 12. Society of Exploration Geophysicists, Tulsa, Oklahoma, USA.

Palmer, D., (1986). Refraction seismics. The lateral resolution of structure and seismic velocity. Geophysical Press Ltd., 269p.

Park, C. B., Miller, R. D., Xia, J., 1999. Multichannel Analysis of surface waves (MASW): *Geophysics*, V. **64,** (3), pp. 800-808.

Pullammanappallil, S., Honjas, W. and Louie, J, N. 2003. Determination of a 1-D shear wave velocities using the refraction microtremor method. *Proc. 3rd Int. Conf. Application of Geophysical Methodologies and NDT to Transportation and Infrastructure,* December 8-12, 2003, Orlando, Florida, USA.

Raines, M.G., D.A. Gunn1, Morgan, D.J.R., Williams, G., Williams, J.D.O. & Caunt, S. 2011. Refraction microtremor (ReMi) to determine the shear wave velocity structure of

the near surface and its application to aid detection of a backfilled mineshaft. *Q.J.E.G.H. (In press)*

Richart F.E. Jr., Wood R.D. & Hall J.R. Jr. (1970). Vibration of soils and foundations. Prentice-Hall, New Jersey.

Rucker, M. L. 2003. Applying the refraction microtremor (ReMi) shear wave technique to geotechnical characterisation. *Proc. 3rd Int. Conf. Application of Geophysical Methodologies and NDT to Transportation and Infrastructure,* December 8-12, 2003, Orlando, Florida, USA.

Seed, R.B., Bray, J.D., Chang, S.W., Dickenson, S.E., 1997. Site dependent seismic response including recent strong motion data. In: Pinto, P.S. (Ed.), Seismic Behaviour of Ground and Geotechnical Structures. A.A. Balkena, Rotterdam, pp. 125–134.

Sensors and Software Inc., Ontariao, Canada.

Skempton, A.W. 1986. Standard Penetration Test Procedures and the Effects in Sands of Overburden Pressure, Relative Density, Particle Size, Aging and Overconsolidation: *Geotechnique*, v. 36:3, p. 425-447

Thomson W.T. 1950. Transmission of elastic waves through a stratified solid medium. *J. Applied Physics*, vol. 21 (1), pp 89-93.

Thorson, J. R., & Claerbout, J. F. 1985.Velocity-stack and slant-stack stochastic inversion. *Geophysics*, 50, pp. 2727-2741

Yuan D. & Nazarian S. 1993. Automated surface wave method: inversion technique. *Jour. Geotech. Eng., ASCE*, vol. 119, (7), pp 1112-1126.

Zagyapan, M. and Fairfield, C.A. (2002). Continuous surface wave and impact methods of measuring the stiffness and density of railway ballast. NDT & E Int. 35, pp75-81.

List of Tables

Table 1. Geotechnical property estimates of the drift and solid geology.

Table 2. Refraction survey over 5 m Bench: Layer designations based on intercept-time calculations.

	Estimates of Geotechnical Properties					
	Unsaturated Deposits			**Saturated Deposits**		
		Shear	**Pressure**		**Shear**	**Pressure**
	Density	**Wave**	**Wave**	**Density**	**Wave**	**Wave**
Lithology		**Velocity**	**Velocity**		**Velocity**	**Velocity**
	(Mgm^{-3})	**(ms^{-1})**	**(ms^{-1})**	**(Mgm^{-3})**	**(ms^{-1})**	**(ms^{-1})**
Sand	1.9	150	350 -500	2.2	150	1600.0
Gravel	1.9	200	400 - 500	2.2	200	1700.0
Mudstone	2.3	800 –	2000 -	2.3	800 –	2000 –

		1000	2500		1000	2500

Table 1. Geotechnical property estimates of the drift and solid geology.

Forward Direction				Depth Calculation using Intercept Velocities						
		Station	Layer 1	Layer 2	Layer 3	Intercept	Intercept	Intercept	Layer 1	Layer 2
	Shot	Position	Velocity	Velocity	Velocity	Layer 1	Layer 2	Layer 3	Thickness	Thickness
	No	(m)	(m/s)	(m/s)	(m/s)	(millisec)	(millisec)	(millisec)	m	m
	3	0	217	451	1482	4.3	32.9	73.7	4.1	8.7
	4	16	145	367	1258	4.8	23.8	66.5	1.9	7.8
	Reverse Direction									
	5	32	173	359	1004	2.5	24.9	62.8	2.4	6.7
	6	48	207	502	1385	7.3	39.0	68.7	4.4	7.1
		Mean	**185**	**420**	**1283**			**Mean SD**	**3.2 1.2**	**7.6 0.9**
		Ratio	**1**	**2.3**	**3.1**					

Table 2. Refraction survey over 5 m Bench: Layer designations based on intercept-time calculations.

List of Figures

a. Refraction superimposed on the radar section.
b. Approx. location (6, 16) on the 2.5 m Grid seismic refraction line.

Fig. 10. Upper refracting horizon w.r.t. bedrock top-surface and structure within HPSG.

a. Upper refraction horizon superimposed on the radar section. Profile along the X=6m section.
b. Continuation of dipping reflector and top of bedrock along X=12m, confirmed via excavation.

Fig. 11. Effect of poor quality phase measurement on the field wavelength calculation.

Fig. 12. Field and inverted CSW data on the 2.5 m Grid compared to penetration resistance.

Fig. 13. Shear wave velocity and penetration resistance profiles of the upper Gunthorpe Formation at location CSW6.

Fig. 14. Field and inverted CSW shear wave velocity profiles on the 5m Grid.

a. CSW3 at position 6m, 24m.
b. CSW5 at position 6m, 48m.

Fig. 15. MASW: Frequency-velocity transform of field record for the 32 m offline shot on the 5 m Grid.

a. Velocity-frequency representation and field record of offline shot.
b. Field record F-K filtered to remove refracted and high order surface waves.

Fig. 16. Dispersion curve picked via MASW in comparison to CSW curve.

a. Channels 3 – 8; about CSW 2.
b. Channels 9 – 15; about CSW 3.
c. Channels 15 – 20; about CSW 4.

Fig. 17. Shear wave velocity-depth profiles via simple MASW and CSW inversions.

a. Channels 3 – 8; about CSW 2.
b. Channels 9 – 15; about CSW 3.
c. Channels 15 – 20; about CSW 4.

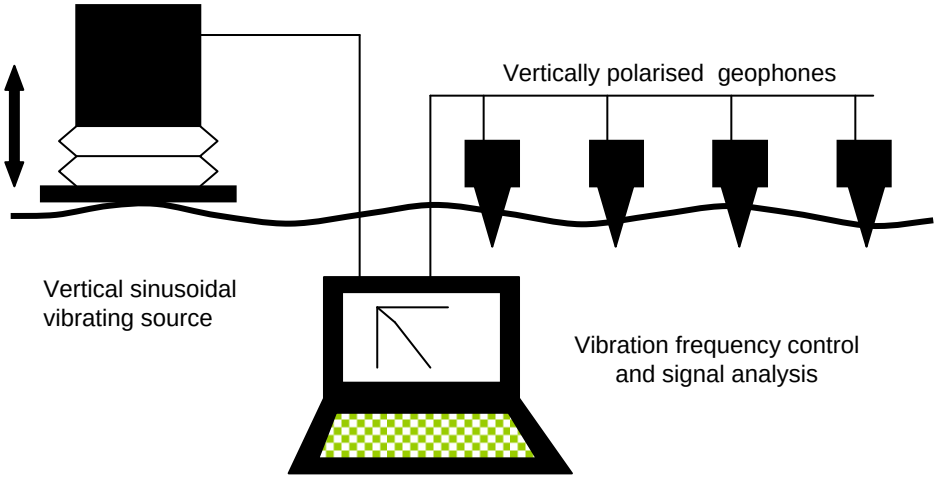

a. Set-up for Continuous Surface Waves (CSW)

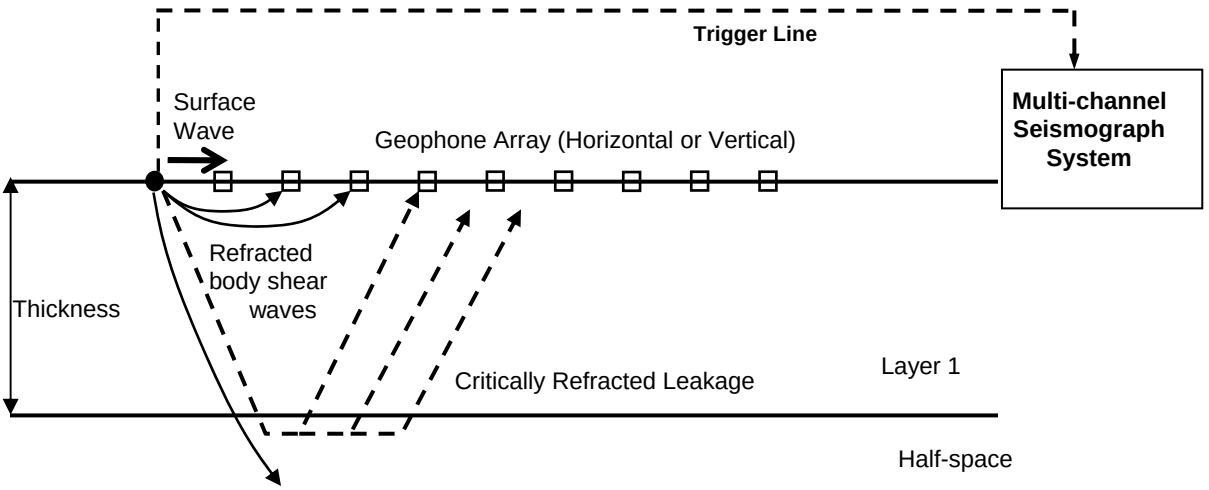

b. Set-up for refraction and multichannel analysis of surface waves methods.

Fig. 1. Schematic of field source-receiver set-ups for different surface wave surveys.

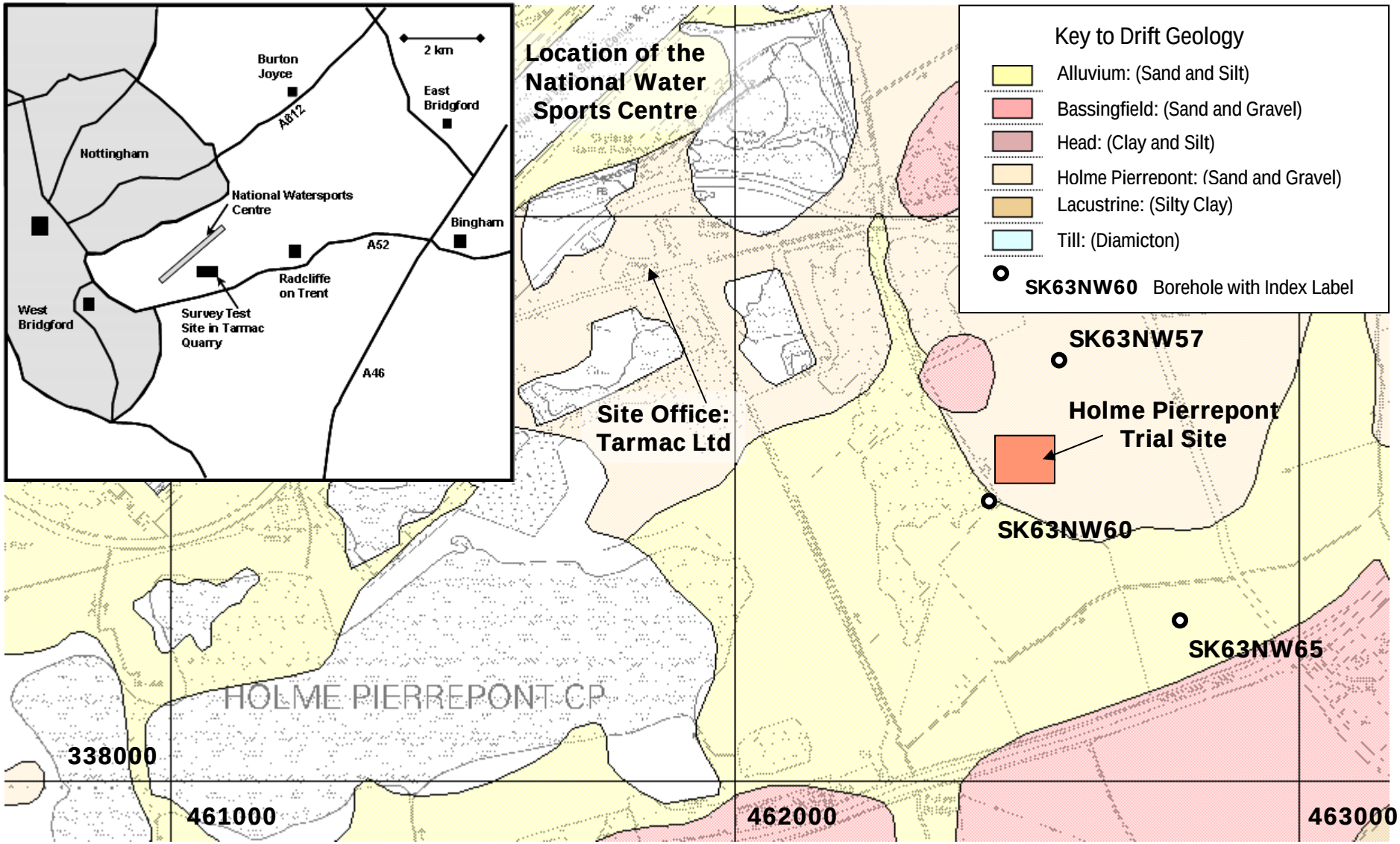

a. Site geographic position relative to surrounding superficial geology and boreholes.

Figure 2. Location and local geology of the Holme Pierrepont trail site.

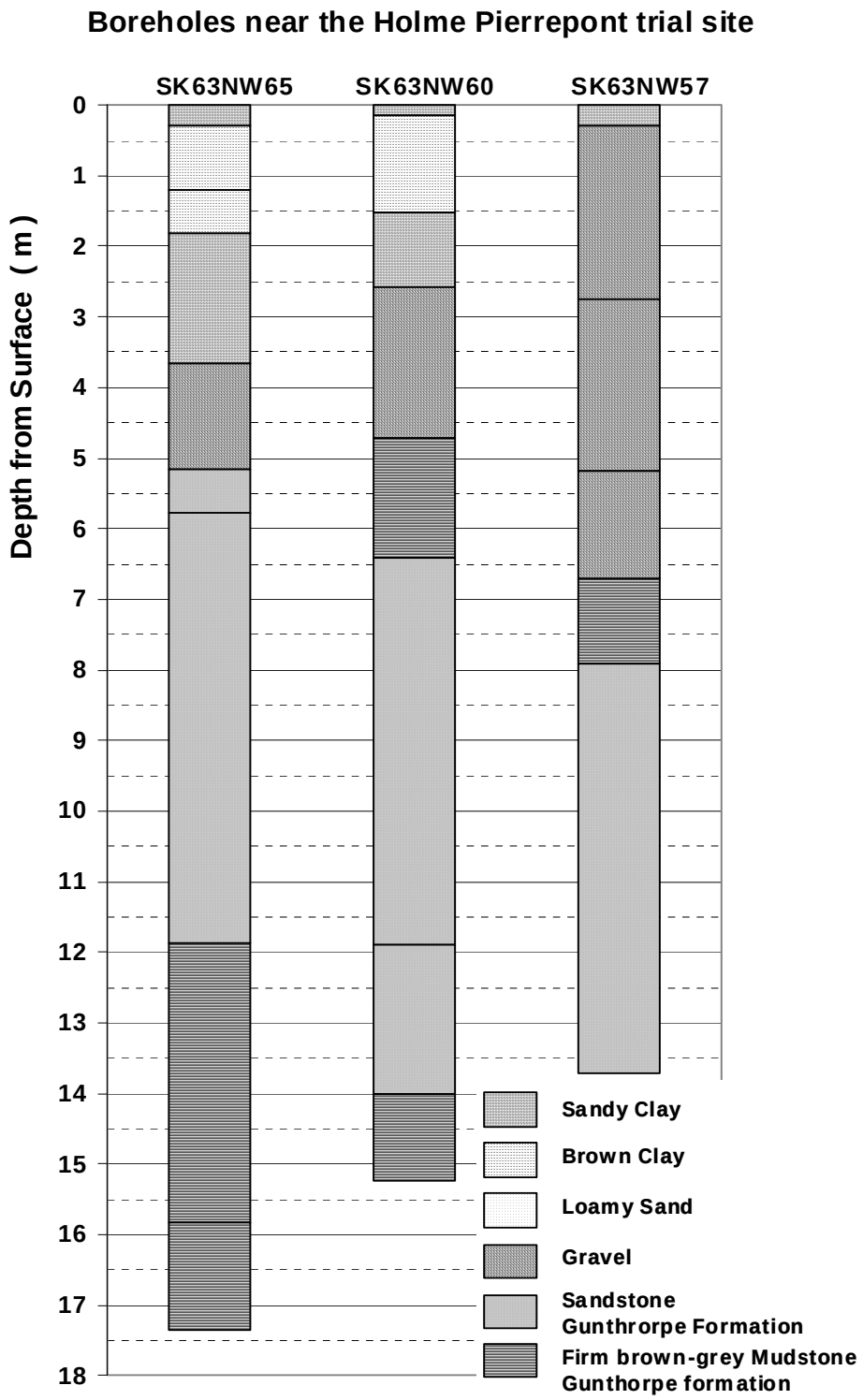

b. Geological logs of boreholes within 500 m of the trial site.

Figure 2. Location and local geology of the Holme Pierrepont trail site.

a. Sub-horizontal, tabular layers with cross-bedding in sand.

b. Channel and bar structures with truncated topsets and preferred orientation in gravel.

Fig. 3. Structure and materials in Holme Pierrepont Sand and Gravels.

a. Top surface hummocky with peak to trough height of approximately 0.5m.

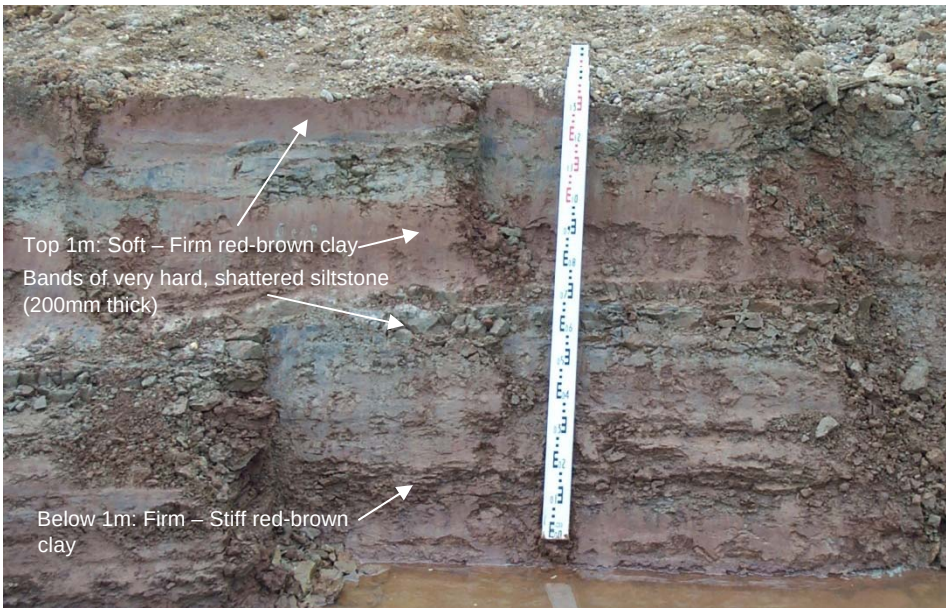

b. Vertical section at the top of the bedrock.

Fig. 4. Structure and materials of the Gunthorpe Formation of the Mercia Mudstone Group

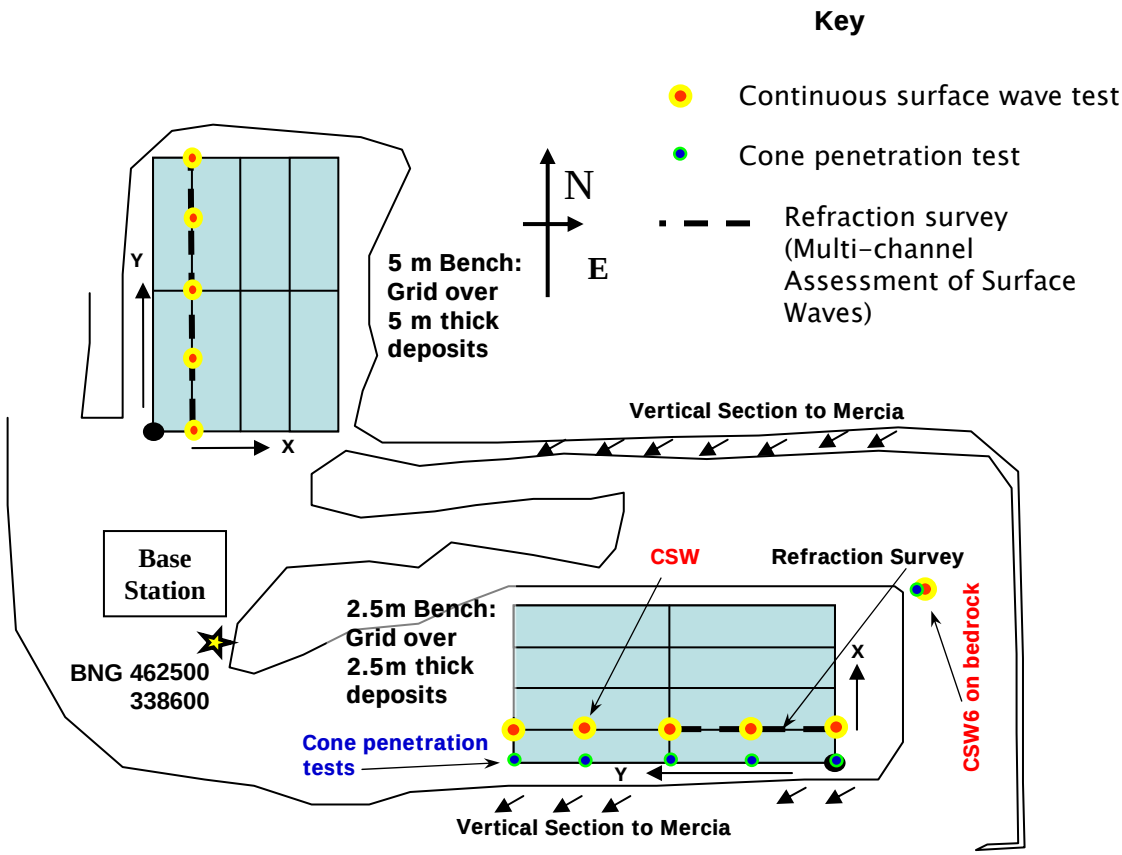

a. Orientation of survey grids.

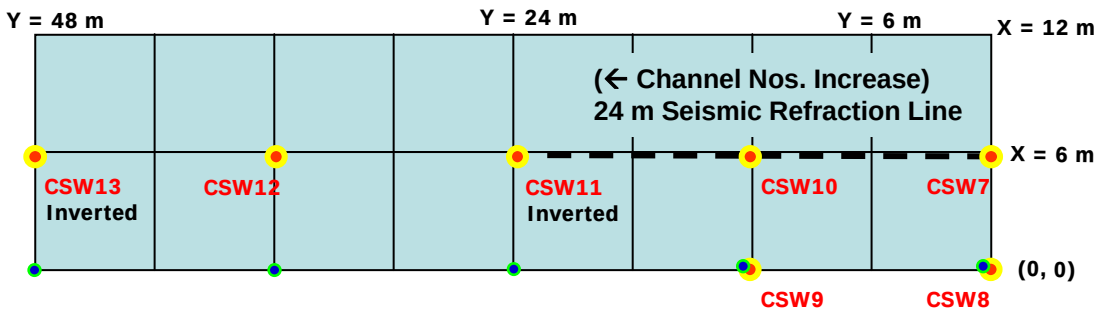

b. Layout of the refraction and CSW surveys over the 2.5 m Bench.

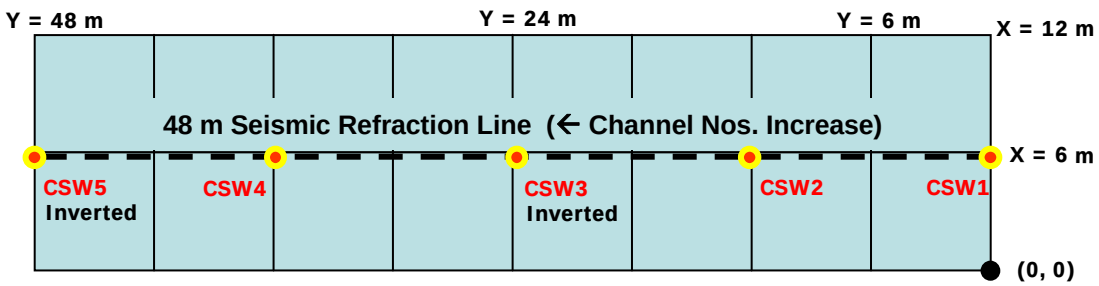

c. Layout of the refraction and CSW surveys over 5 m Bench.

Fig. 5. Orientation and layout of surface wave surveys.

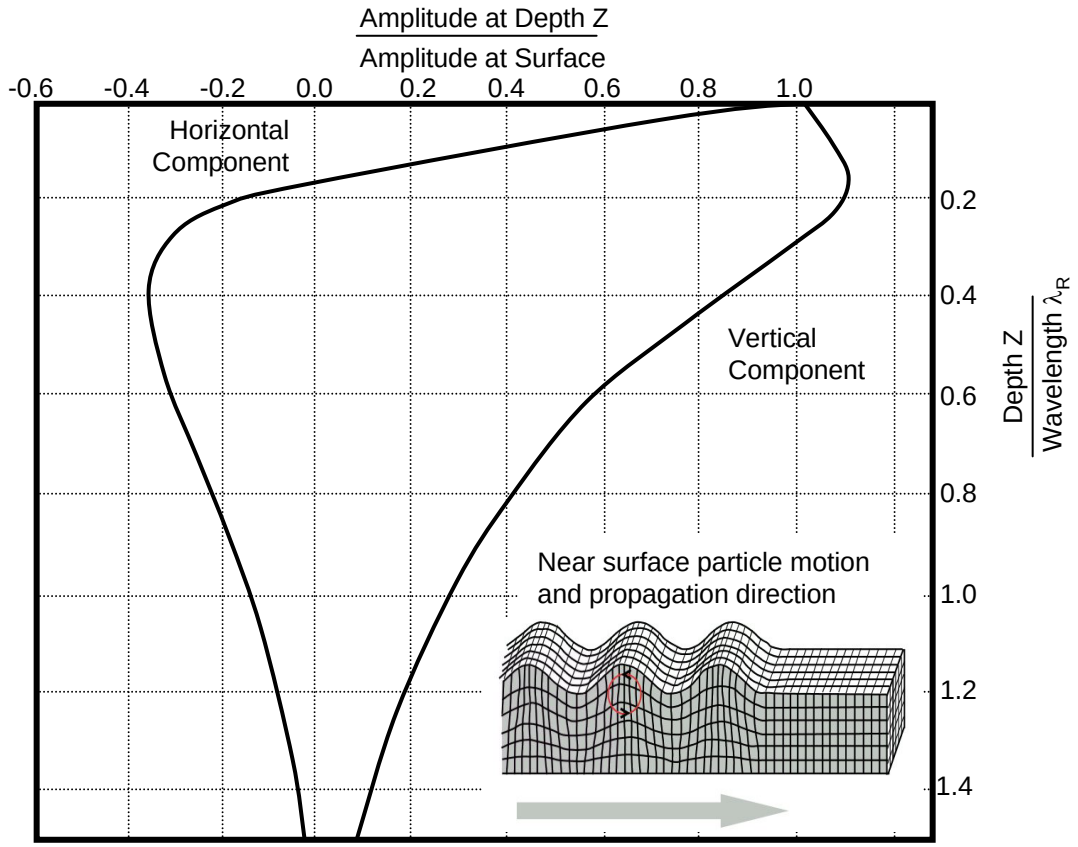

a. Rayleigh wave: near surface particle motion tacks a retrograde ellipse.

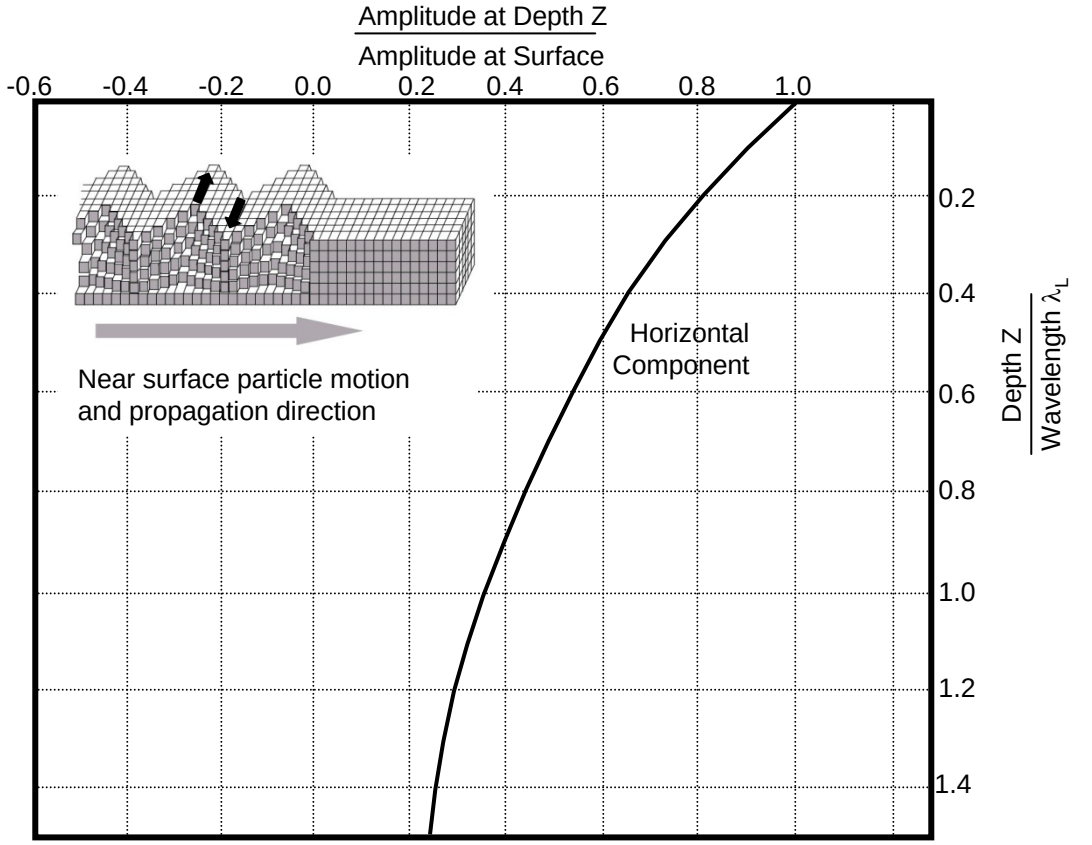

b. Love wave: transverse, horizontally polarised near surface particle motion.

Figure 6. Fundamental surface wave particle motion and the amplitude of the vertical / horizontal components versus dimensionless depth, (modified after Richart *et al.* 1970).

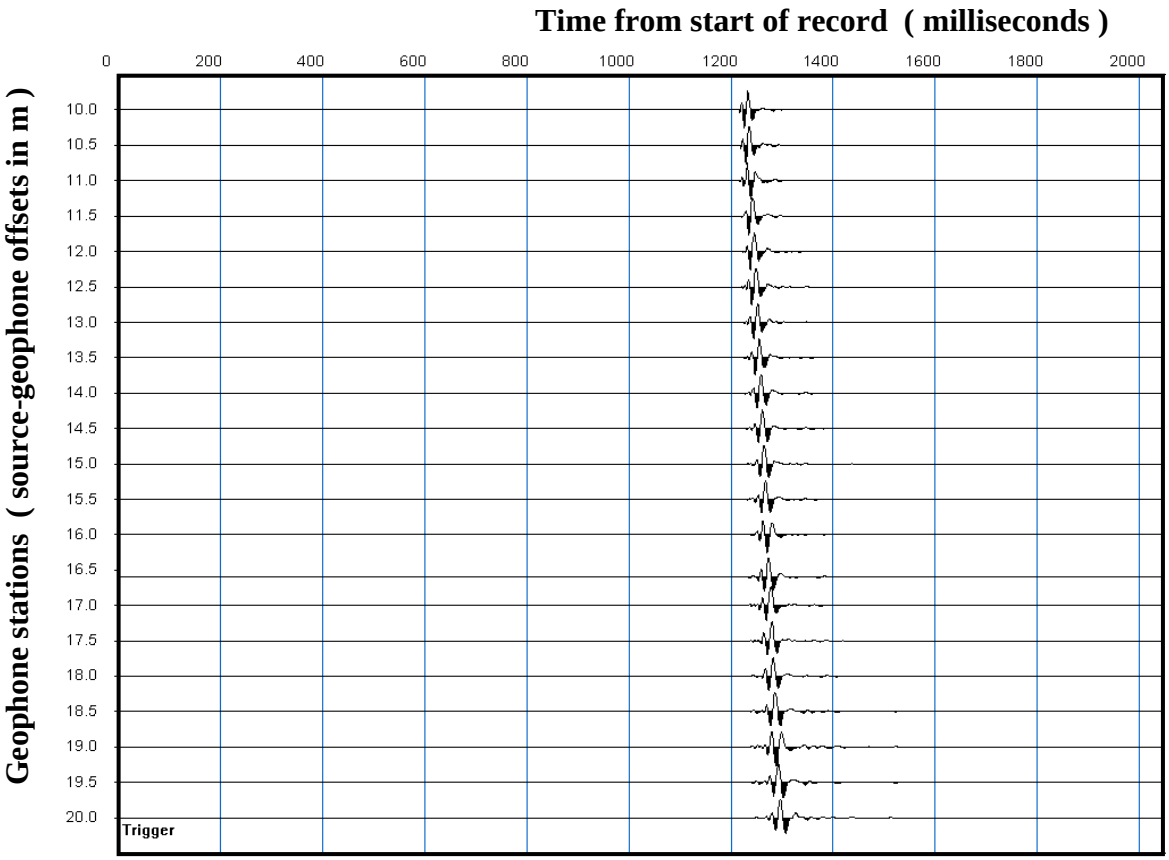

a. Surface wave disturbance on field trace.

Fig. 7. Transformation of field seismic record into a phase velocity dispersion curve.

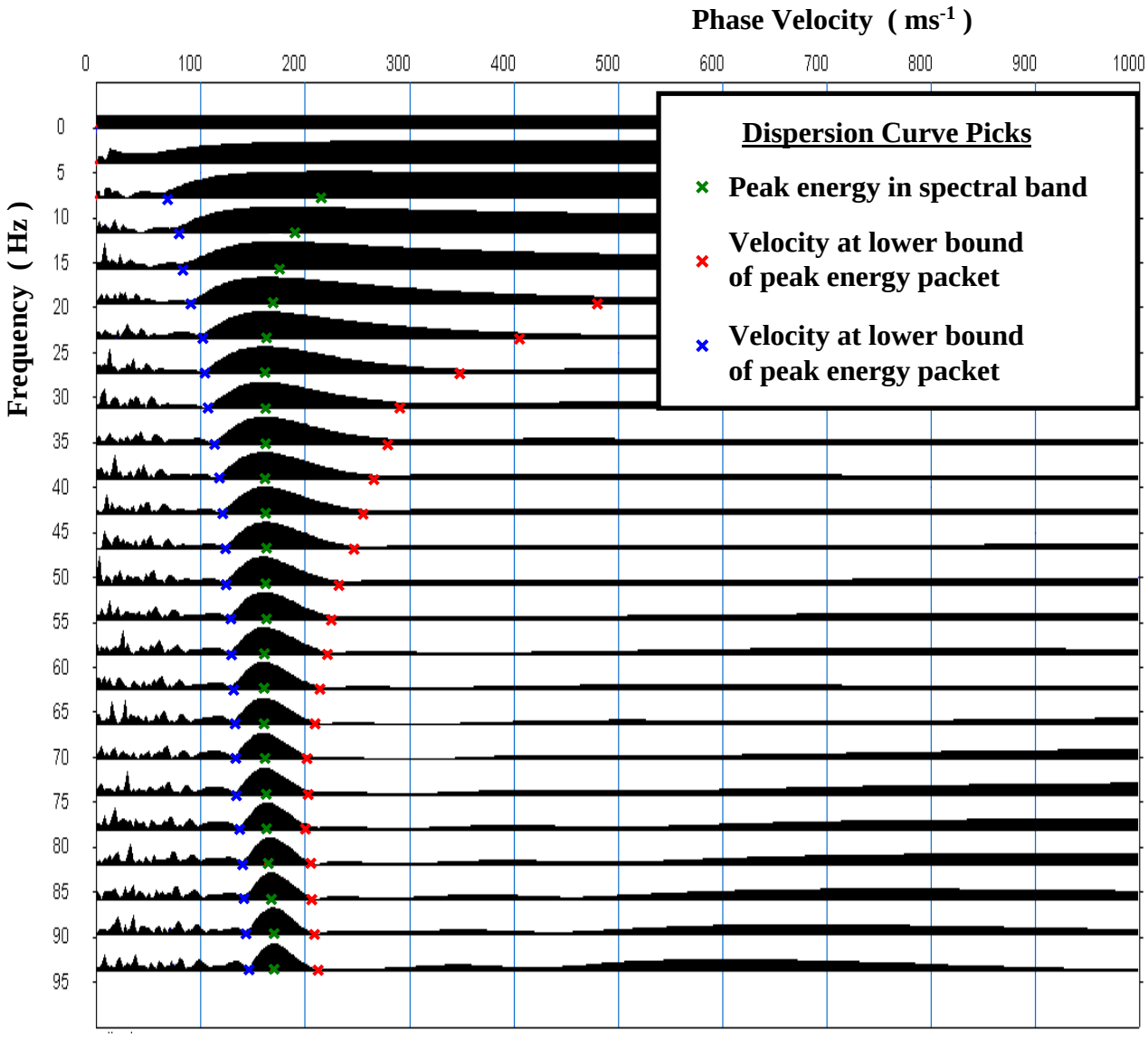

b. Phase velocity-frequency transformation.

Fig. 7. Transformation of field seismic record into a phase velocity dispersion curve.

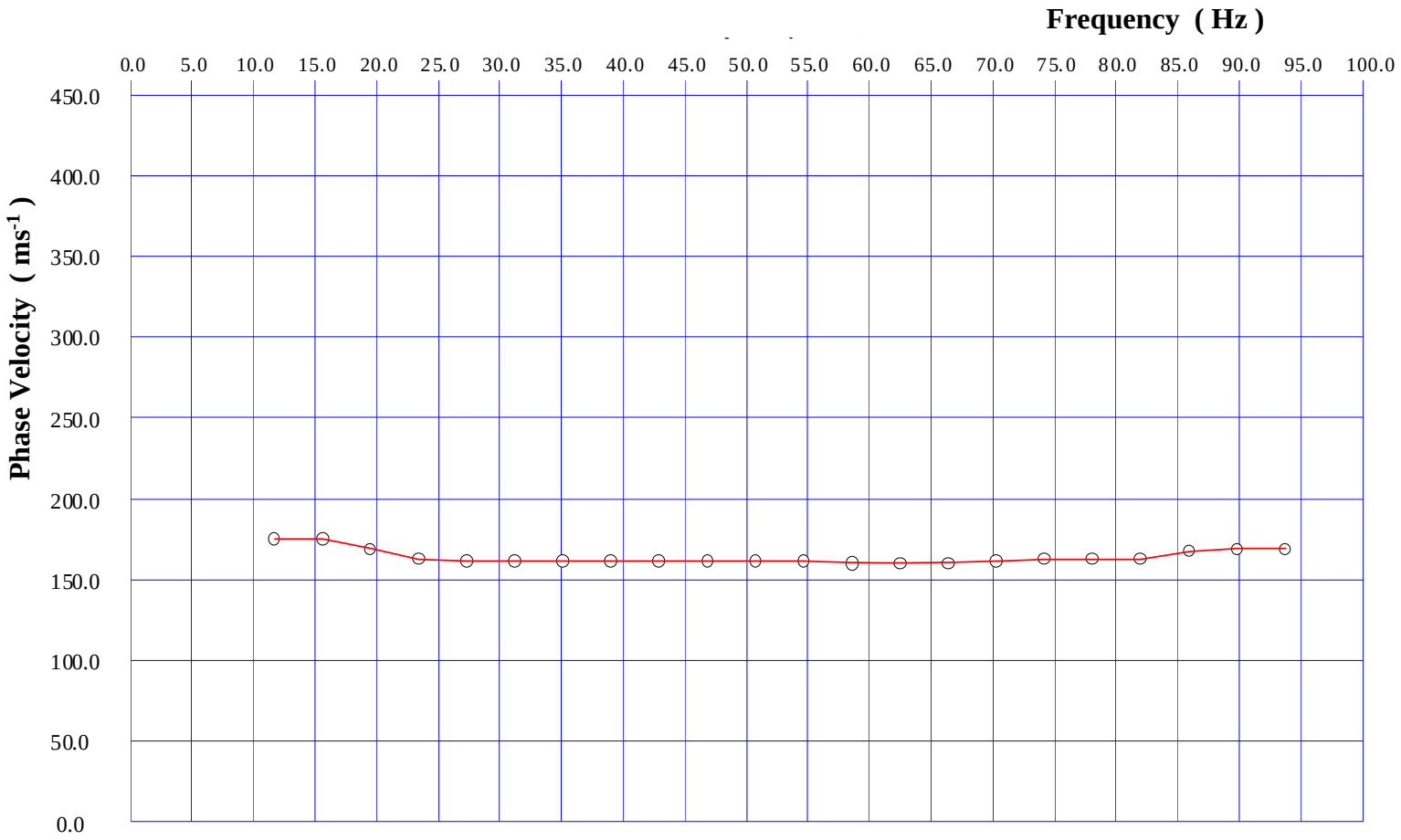

c. Phase velocity dispersion curve picked from the peak energy in spectral band.

Fig. 7. Transformation of field seismic record into a phase velocity dispersion curve.

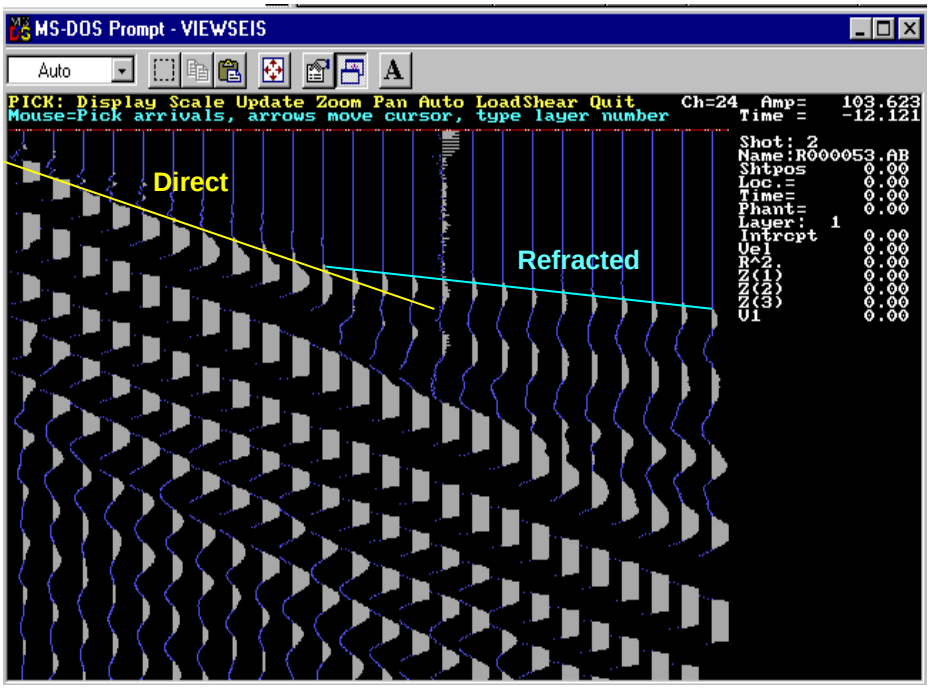

a. Direct and refracted events from endline shot.

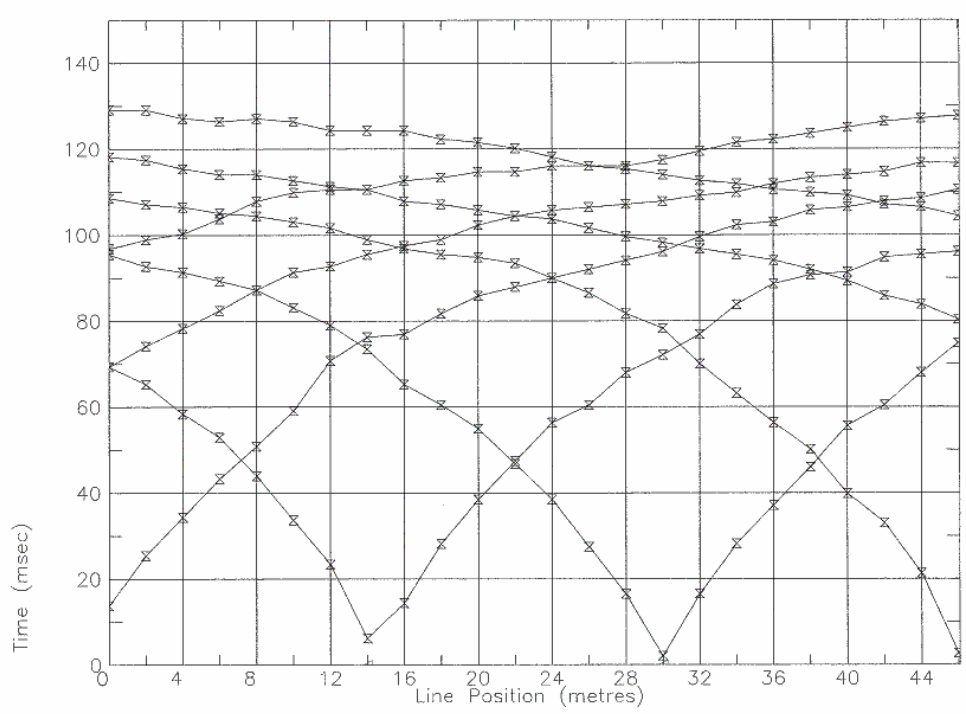

b. 5 m Bench: Time-distance plot of first arrival picks.

Fig. 8. Example of field record and time-distance interpretation of the refraction surveys.

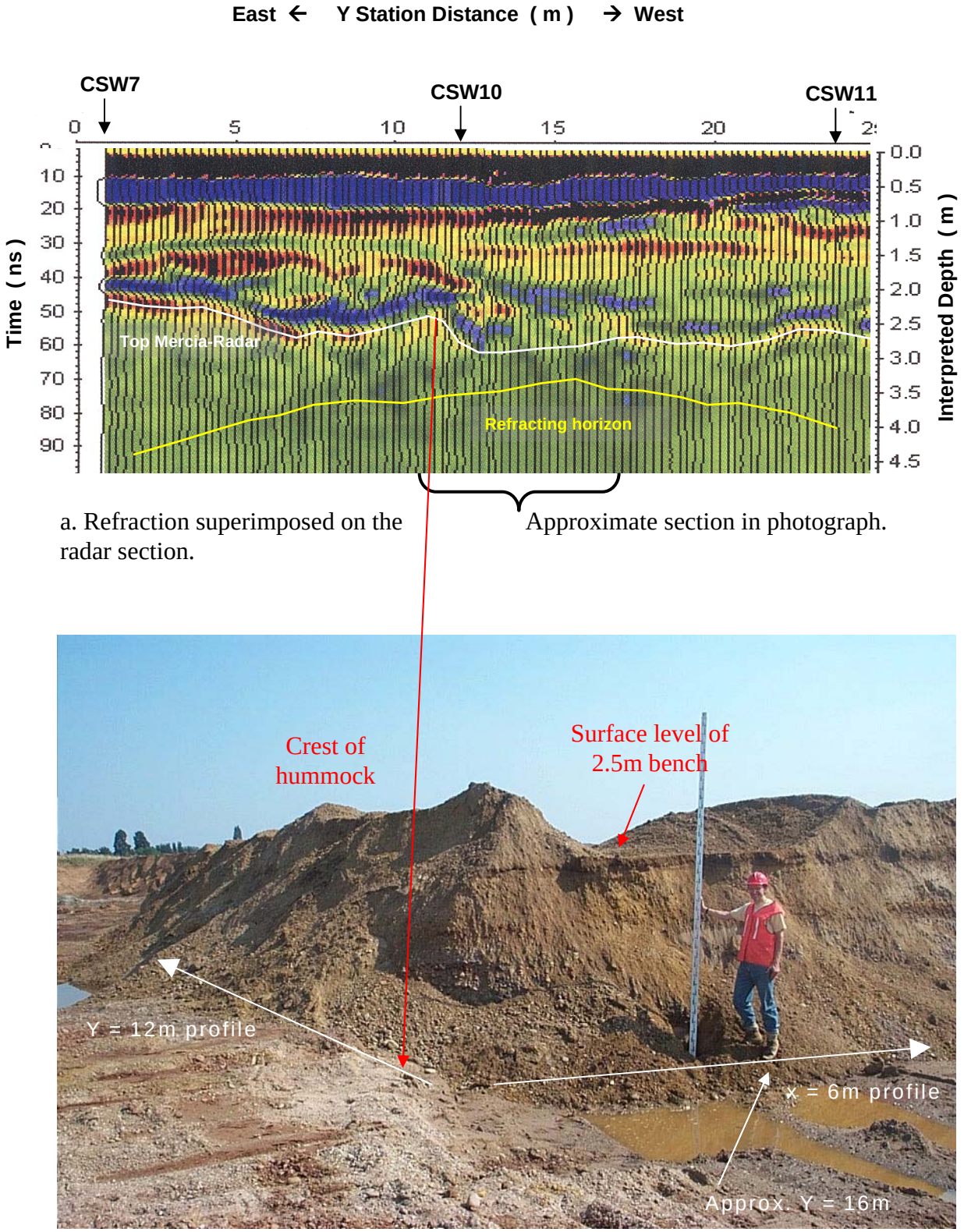

a. Refraction superimposed on the radar section.

Approximate section in photograph.

b. Approx. location (6, 16) on the 2.5 m Grid seismic refraction line.
Top of Mercia Mudstone hummocky: peak to trough height approx 0.5m.
Protective artificial bank cleared to approx. top surface level of the bench.

Fig.9. Refracting horizon over the 2.5 m Bench relative to bedrock top-surface.

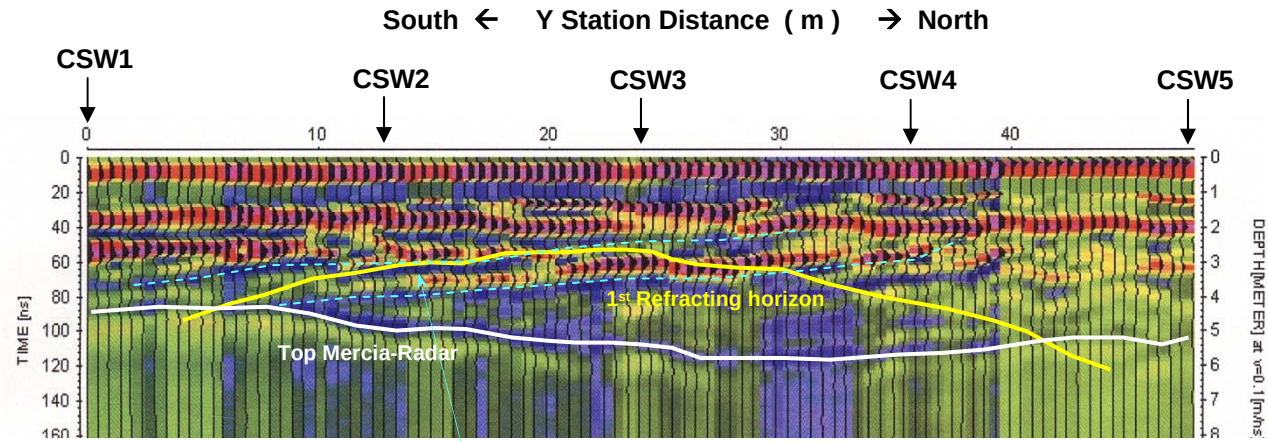

a. Upper refraction horizon superimposed on the radar section. Profile along the X=6m section.

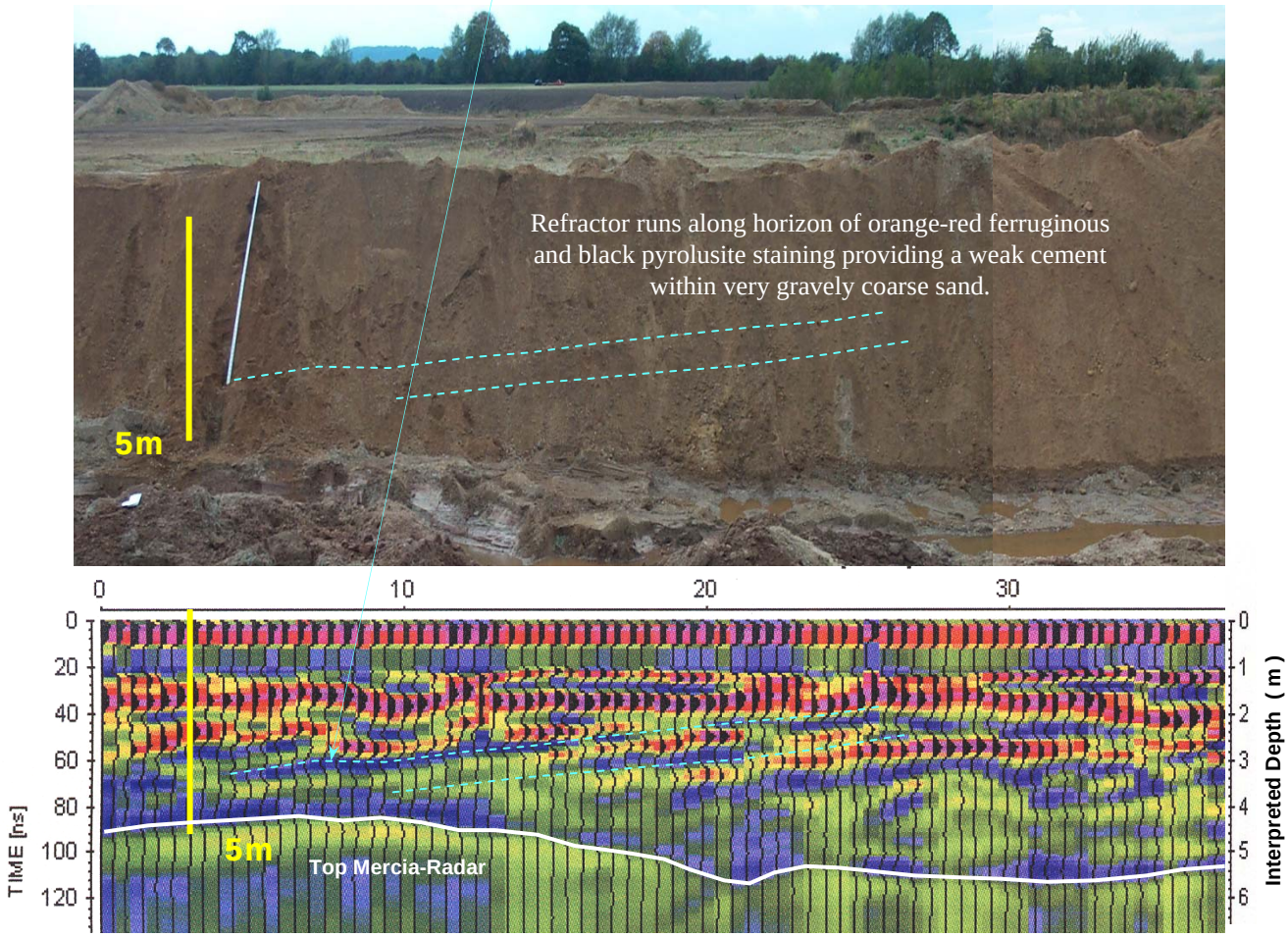

b. Continuation of dipping reflector and top of bedrock along X=12m, confirmed via excavation.

Fig. 10. Upper refracting horizon w.r.t. bedrock top-surface and structure within HPSG.

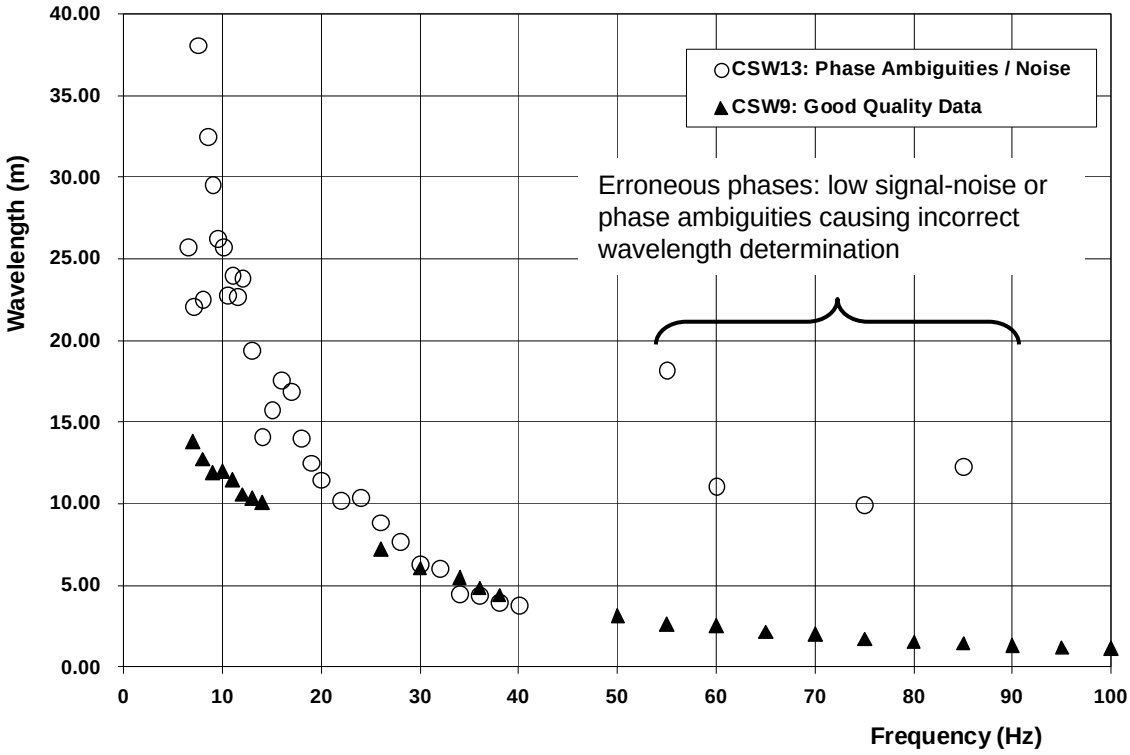

Fig. 11. Effect of poor quality phase measurement on the field wavelength calculation.

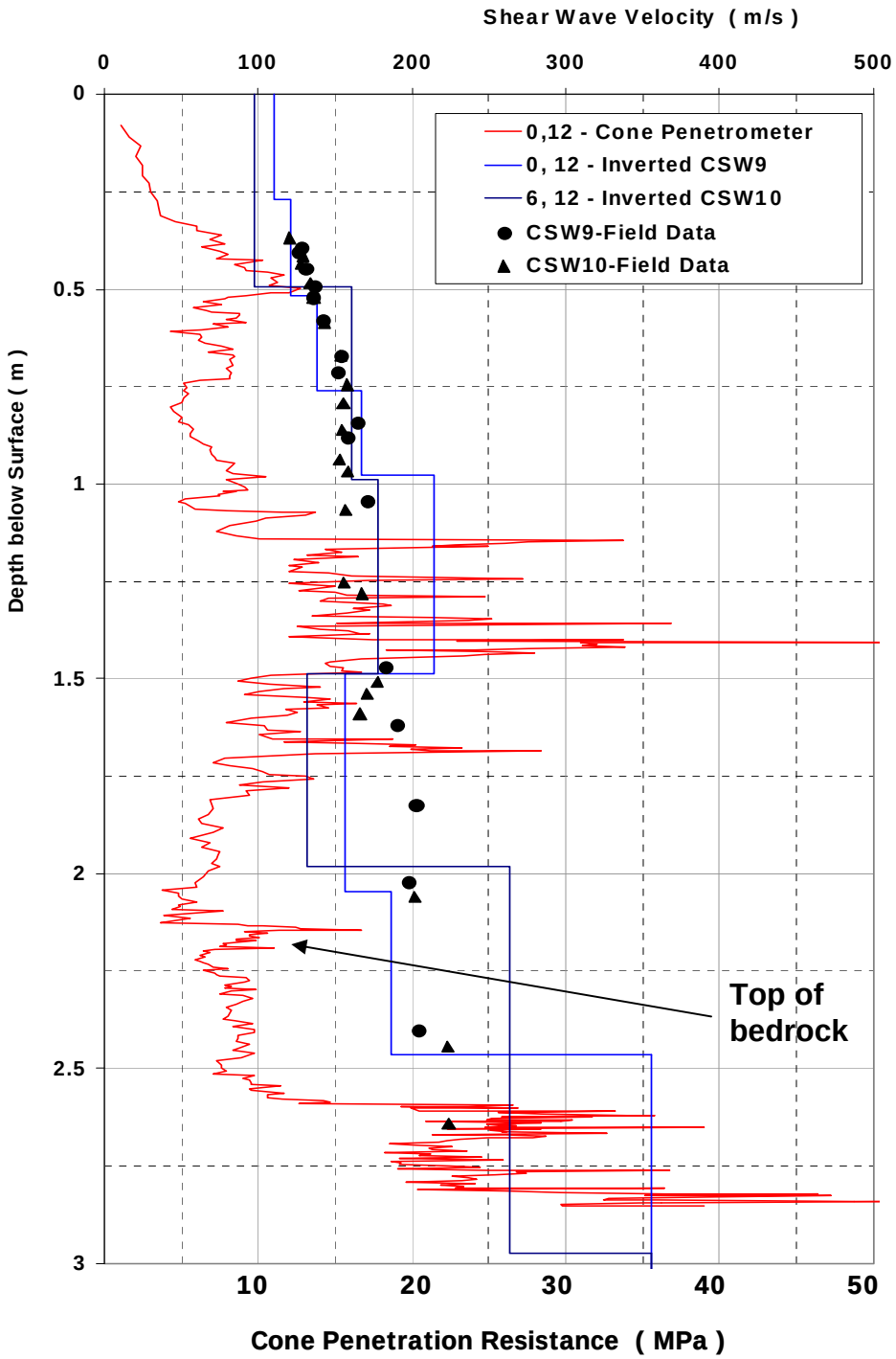

Fig. 12. Field and inverted CSW data on the 2.5 m Grid compared to penetration resistance.

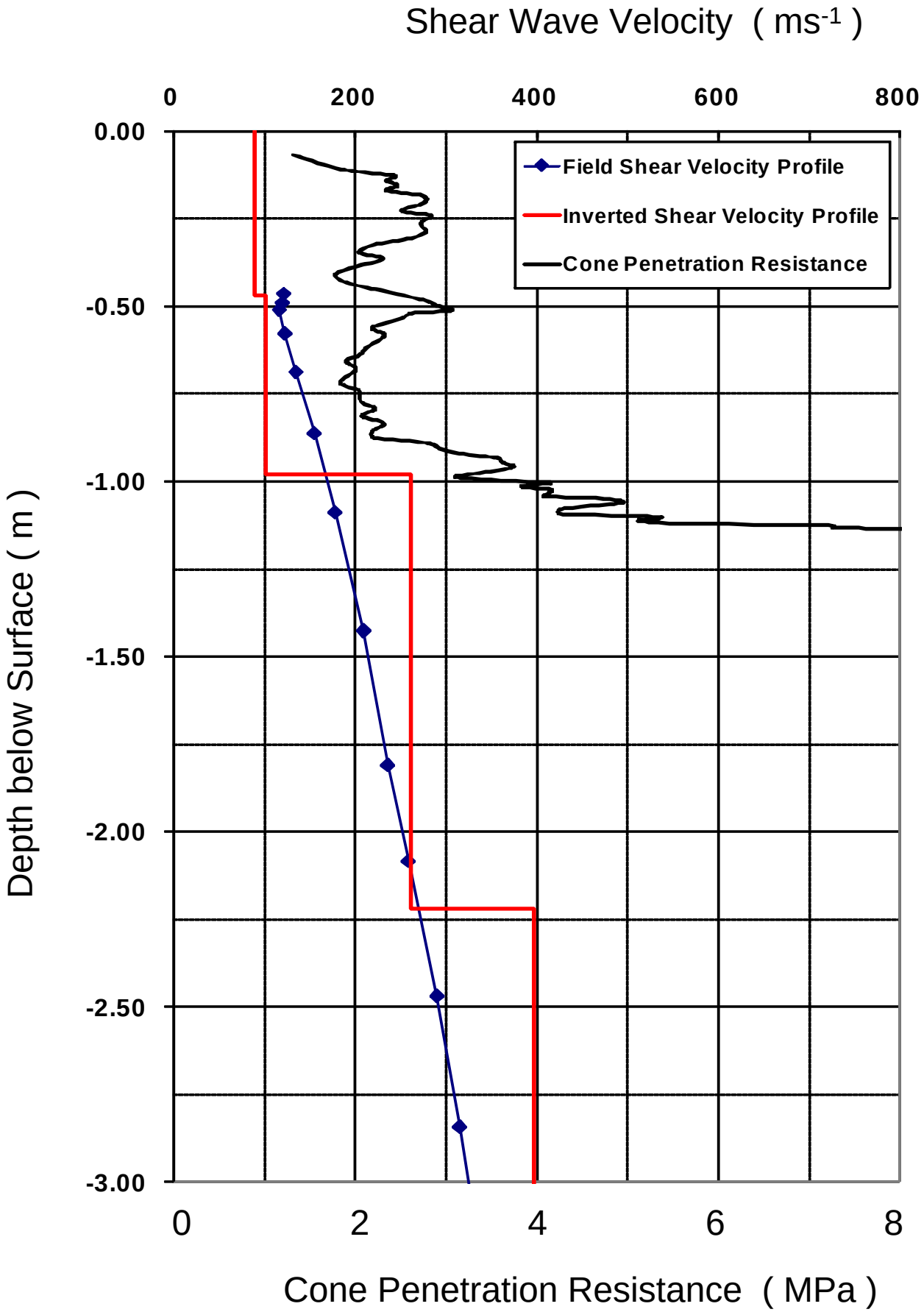

Fig. 13. Shear wave velocity and penetration resistance profiles of the upper Gunthorpe Formation at location CSW6.

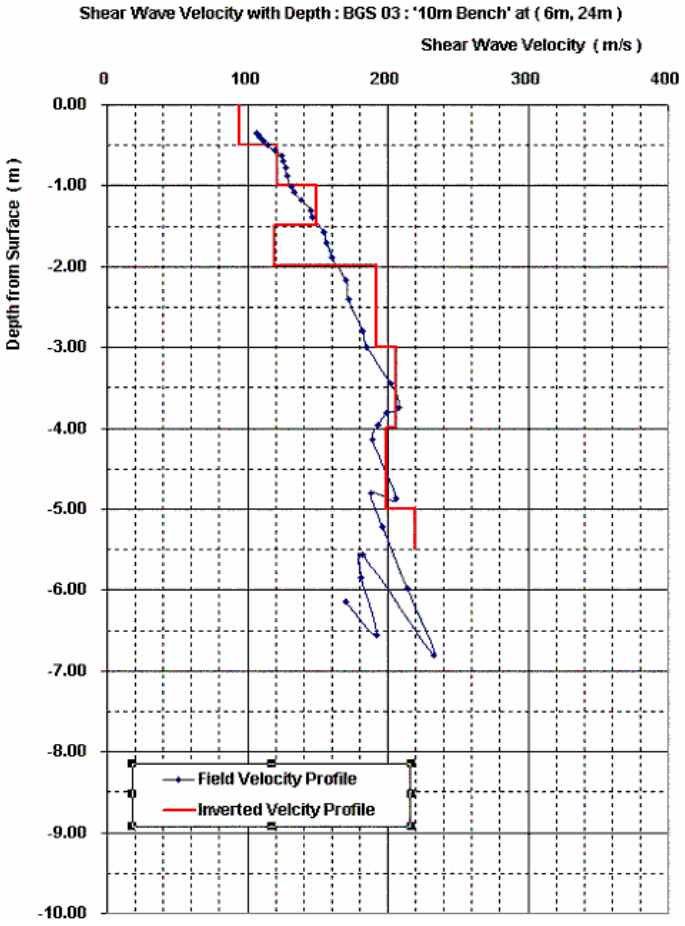

a. CSW3 at position 6m, 24m.

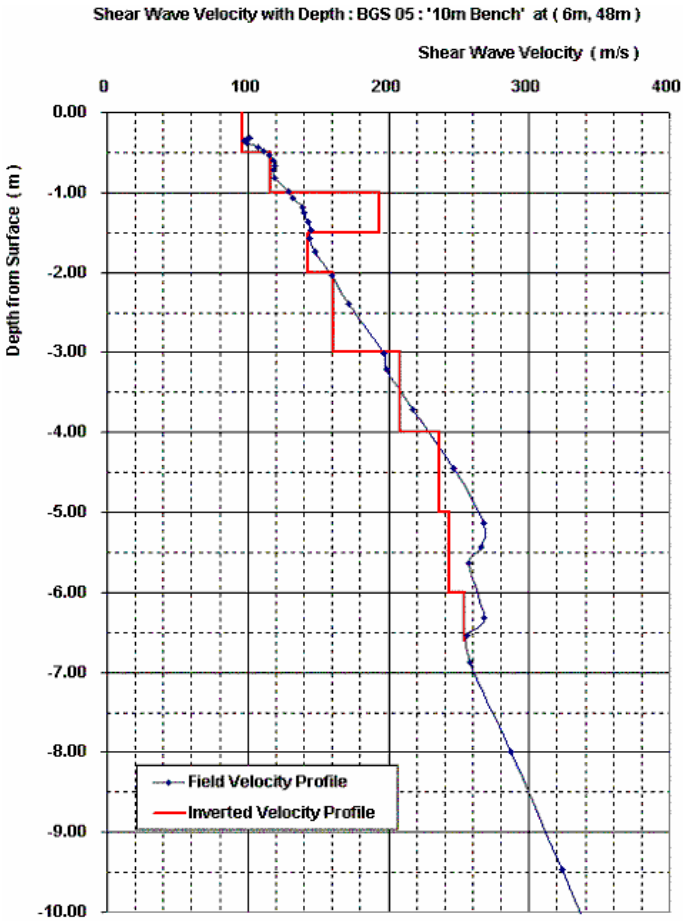

b. CSW5 at position 6m, 48m.

Fig. 14. Field and inverted CSW shear wave velocity profiles on the 5m Grid.

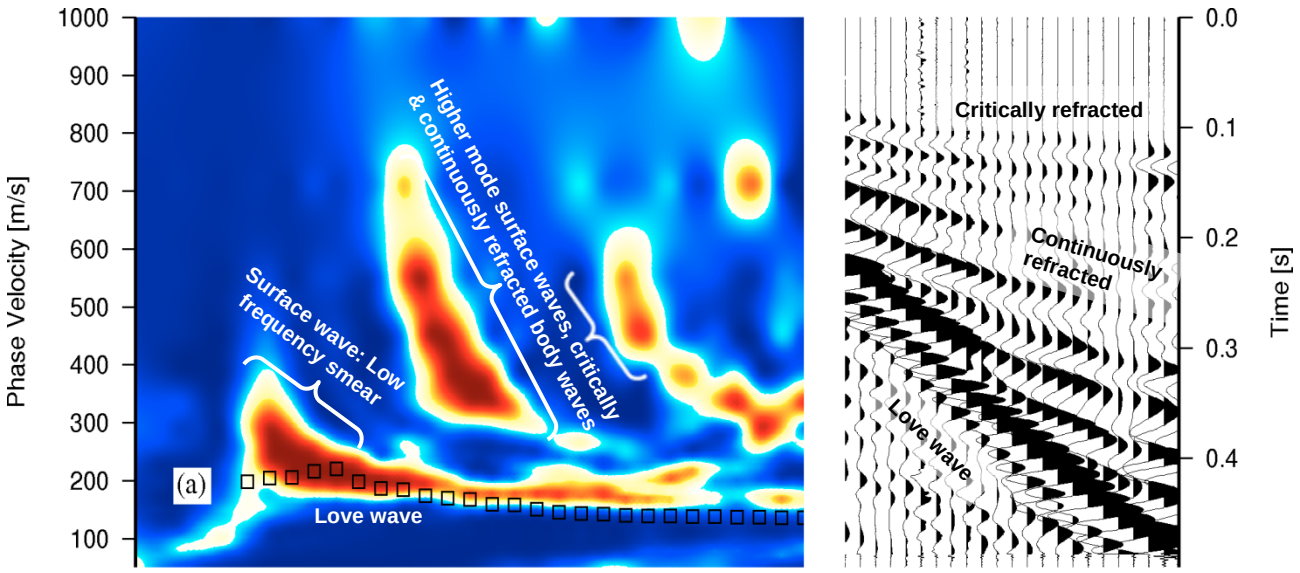

a. Velocity-frequency representation and field record of offline shot.

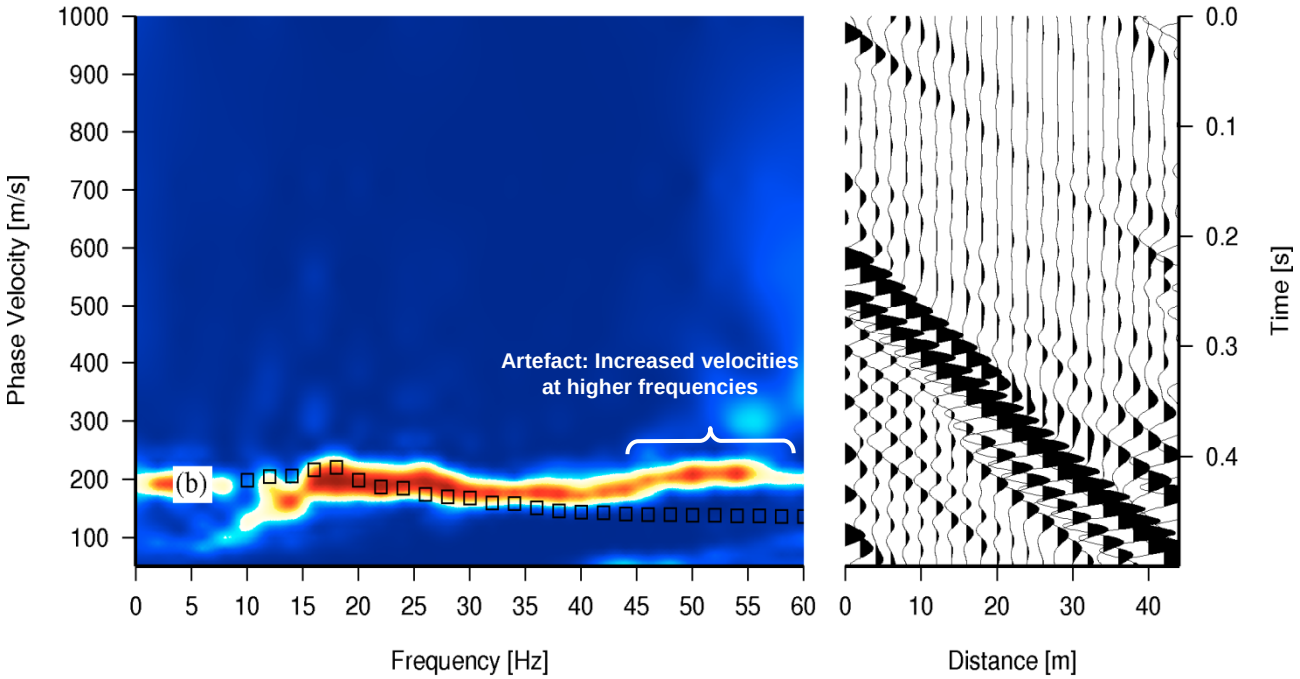

b. Field record F-K filtered to remove refracted and high order surface waves.

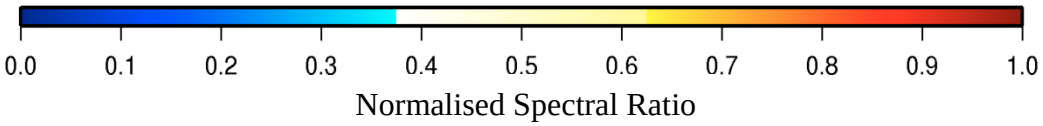

□ Plot of dispersion curve from CSW3 in the middle of the array.

Fig. 15.MASW: Frequency-velocity transform of field record for the 32 m offline shot on the 5 m Grid.

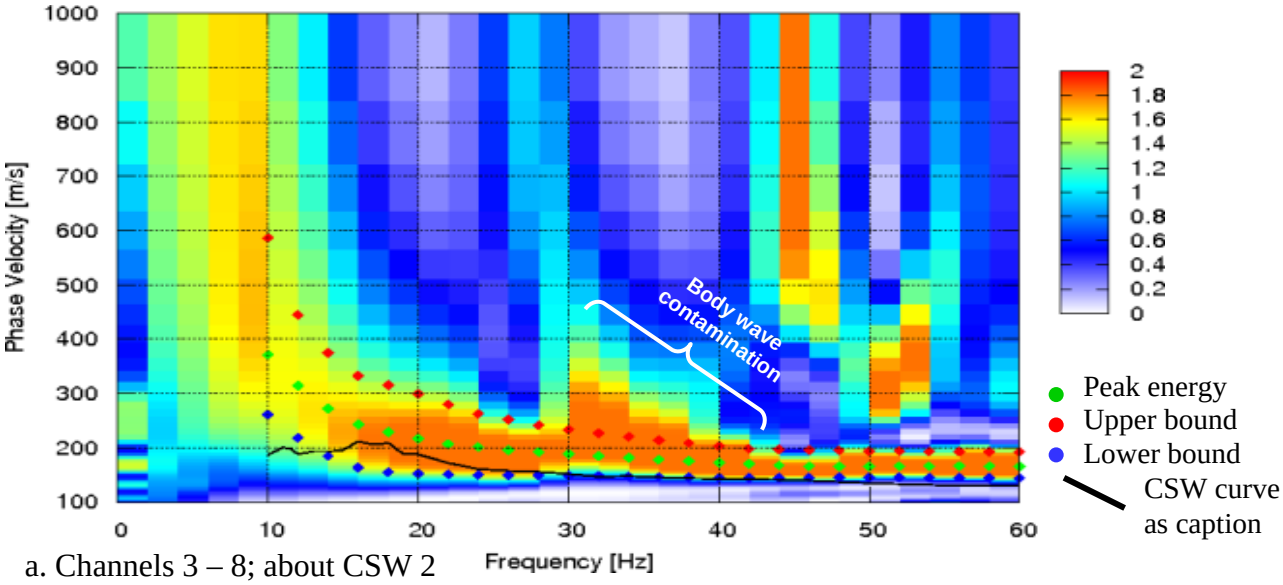

a. Channels 3 – 8; about CSW 2

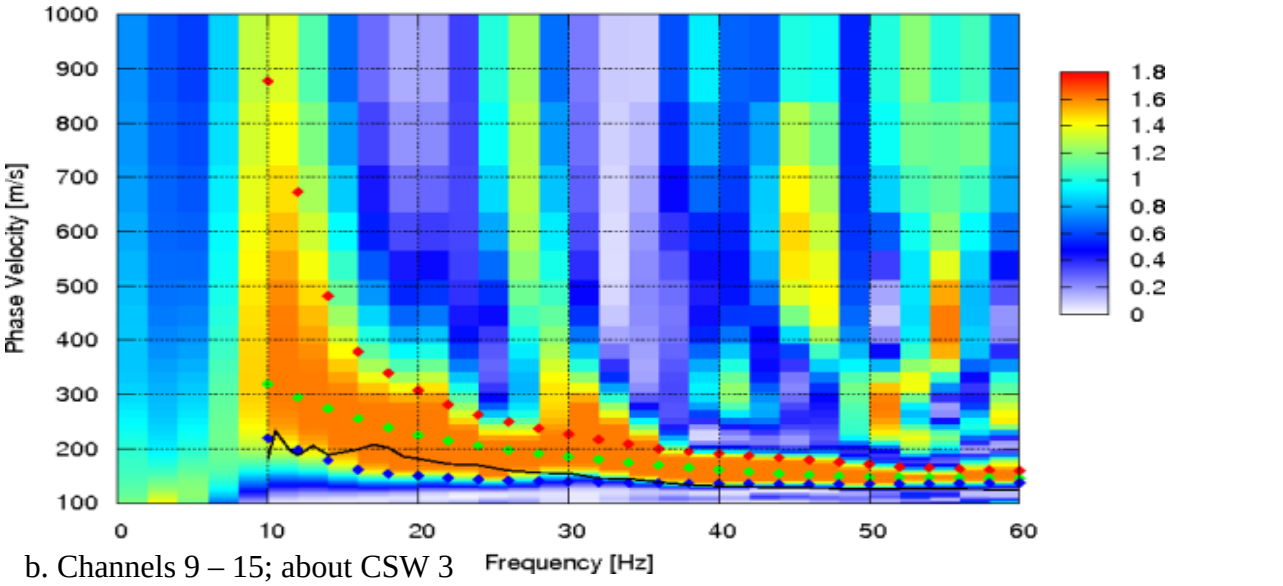

b. Channels 9 – 15; about CSW 3

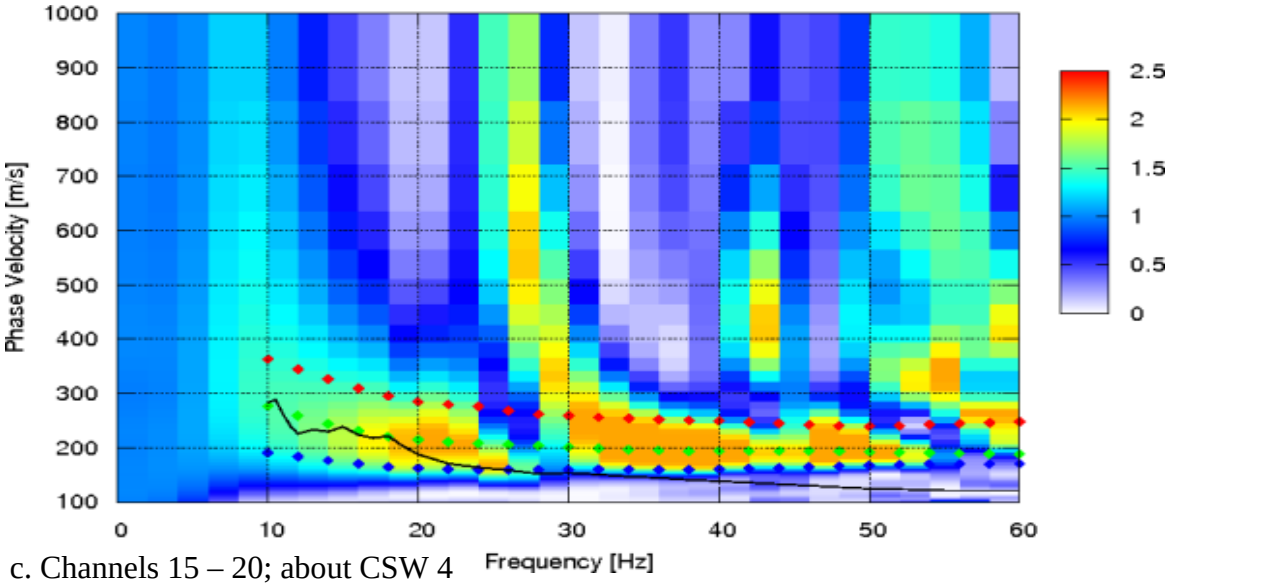

c. Channels 15 – 20; about CSW 4

Fig. 16. Dispersion curve picked via MASW in comparison to CSW curve.

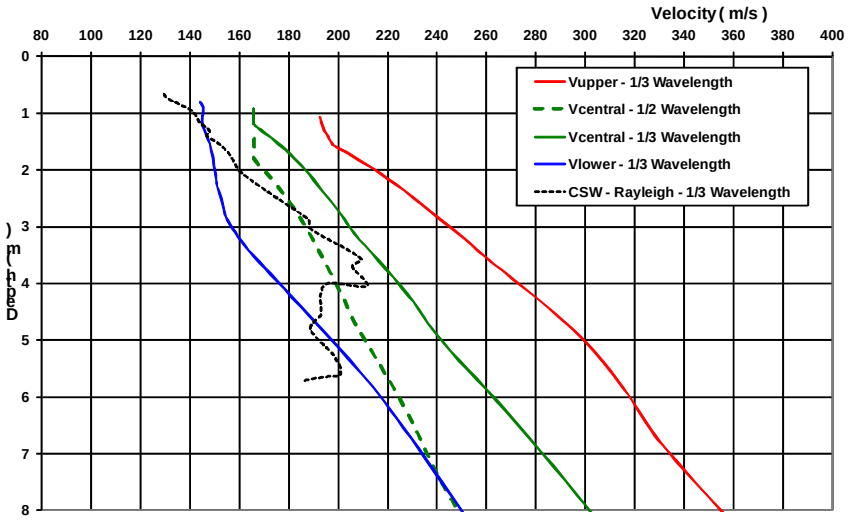

a. Channels 3 – 8; about CSW 2

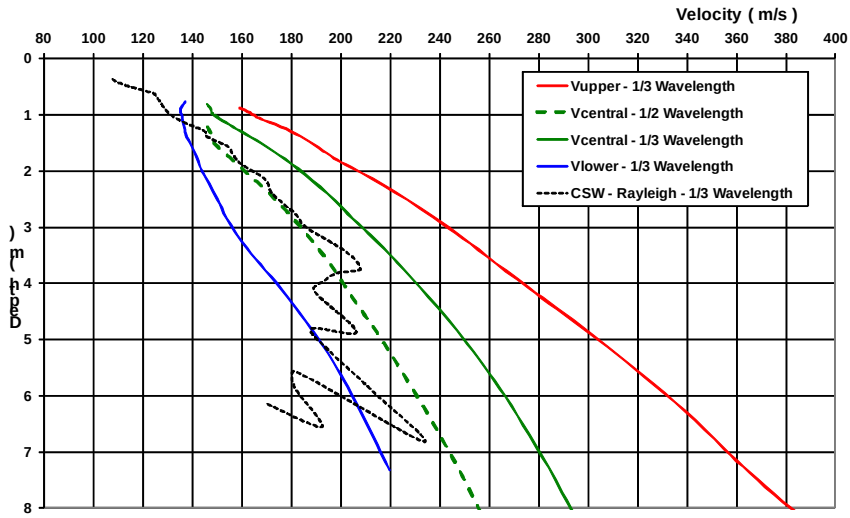

b. Channels 9 – 15; about CSW 3

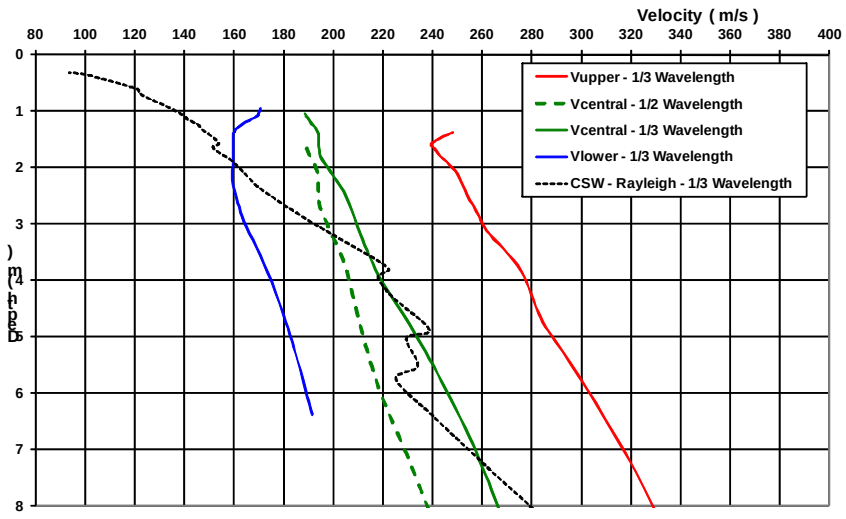

c. Channels 15 – 20; about CSW 4

Fig. 17. Shear wave velocity-depth profiles via simple MASW and CSW inversions.